Characterization Techniques for Hybrid Nanocomposites Based on Graphene and Nanoparticles

Mohamed Hamid Salim, Zineb Kassab, Ihsane Kassem, Houssine Sehaqui, Rachid Bouhfid, Johan Jacquemin, Abou El Kacem Qaiss, Jones Alami, and Mounir El Achaby

Abstract Hybrid nanocomposites have appealing chemical and physical properties and are used on a large scale worldwide. Graphene-nanoparticles (G-NP) hybrid fillers and their composites have particularly gained attention among researchers in recent times, as the incorporation of nanoparticles (NP) into the chemically derived graphene (G) in hybrid fillers open for new applications. This is as a result of the synergetic properties of the obtained materials, such as biodegradability, low density, physical and chemical structure, etc. The novelty of this chapter is to present a review of the recent studies of G-NP hybrid filler's characteristics and their composites using the most fundamental characterization techniques. Our literature review examines various published findings regarding, among others, surface, mechanical and thermal properties in order to determine the performance of the fillers. Therefore, we briefly reviewed their basic structure and surface modifications of G-NP hybrid fillers and nanocomposites. The main output is to study and review techniques frequently reported in the literature to examine their structure and properties, we exemplified and discussed in this chapter key results collected from SEM, AFM, TEM, HRTEM, FTIR, UV-vis, Raman, XRD, XPS, SEM, TGA-DTA, DMA and tensile analyses. To help the readers, this chapter is subdivided into three sections covering a state-of-the-art of the most recent hybrid fillers, their preparation and characterization. The overall objective of this chapter is to dress a relationship between their structure and property to provide key indicators and future directions for their efficient large-scale

M. H. Salim · Z. Kassab · I. Kassem · H. Sehaqui · J. Jacquemin · J. Alami · M. El Achaby (✉)
Materials Science and Nano-engineering (MSN) Department, Mohammed VI Polytechnic University (UM6P), Lot 660 – Hay Moulay Rachid, 43150 Benguerir, Morocco
e-mail: mounir.elachaby@um6p.ma

R. Bouhfid · A. E. K. Qaiss
Composites and Nanocomposites Center (CNC), Moroccan Foundation for Advanced Science, Innovation and Research (MAScIR), Rabat Design Center, Rue Mohamed El Jazouli, Madinat El Irfane, 10100 Rabat, Morocco

J. Jacquemin
Laboratoire PCM2E, Faculté des Sciences, Université de Tours, Parc Grandmont, 37200 Tours, France

A. E. K. Qaiss et al. (eds.), *Graphene and Nanoparticles Hybrid Nanocomposites*, Composites Science and Technology,
https://doi.org/10.1007/978-981-33-4988-9_2

production of G-NP hybrid nanocomposite with unique characteristics for different applications.

1 Introduction

Research on nanomaterials characteristics and properties has seen a strong increase thanks to the ever-increasing industrial needs [1], and the limited performance of conventional materials [2, 3]. The hybridization of different materials at the nanometer scale has been shown to bring about new and improved materials properties [4]. Among those, graphene (G) with its derivatives (graphene oxide (GO), reduced graphene oxide (rGO) and graphene oxide nanosheets (GON)) combined with nanoparticles (NP) have been developed as novel hybrid nanomaterials with excellent properties [5, 6].

Since its discovery, G is at the forefront of research in various fields of application because of its excellent chemical, electrical, optical and mechanical properties. It was proposed for applications such as a nanofiller in hybrid nanocomposites [7, 8], consisting of functional inorganic nanoparticles or aggregates incorporated in a polymer matrix. These materials exhibit several distinctive properties that are not achievable with organic polymers or inorganic materials individually. The G-NP based polymeric composites have excellent properties like mechanical, thermal, optical, and structural which are not observed in bulk materials [9–11]. Additionally, the performance of hybrid polymer nanocomposite is dependent on the characteristics of hybrid nanofillers, the filler dispersion in the matrix, the interlinkages linking the matrix and the arrangement of fillers within the matrix [12–14]. In recently published works, it has been demonstrated that G-NP based hybrid composite nanomaterials are ideal for use in different applications, such as food packaging, energy storage, sensors technology, water treatment, and transparent-flexible electrodes [15–17].

Hence, there is a need to understand the characteristics of the different G-NP hybrids like their morphology, the choice to incorporate organic or inorganic materials dispersed in the polymer matrix, which can lead to several changes in properties of the neat material. Therefore, in order to facilitate a better understanding of the characteristics of the G-NP based materials, for the first time, this chapter reviewed and classified the G-NP hybrids into five categories: (1) G-metal and metal oxide, (2) G-metal alloy, (3) G-carbon nanotubes, (4) G-nanocellulose and v) G-nanoclays.

Metal or metal oxide nanoparticles are commonly used to produce the G-based hybrid nanofillers [18]. G hybrids incorporated with different metal nanoparticles have been reported like, for example, G-Au [19], G-Ag [20], G-Cu [18], G-Ni [21], G-Pd [22], G-Zn [23], etc. Besides, there are numerous G-metal and G-metal-oxide nanohybrid synthesis methods. Similarly, various nanometal alloys were integrated by appropriate synthetic approaches on the G surface to ensure a high degree of morphological and structural properties and minimizing the possibility of their fragmentation and agglomeration in the matrix [18, 24, 25]. Currently, researchers have developed different synthetic methods for the preparation of the G-metal alloy

nanohybrids, such as reduction, solvothermal, microwave-assisted, electrochemical and chemical vapor deposition [25–28].

Recently, carbon nanomaterials, such as carbon nanotubes (CNT), were introduced to the carbon family. Carbon nanotubes (both single- and multi-walled CNT) with G are commonly used as nanofillers of polymer composite materials [29, 30]. Various processes including chemical vapor deposition, physical vapor deposition, chemical processing, pyrolysis, 3D printing and more assembly-based techniques were developed to produce 3D G-CNT materials [10, 31–33]. G and CNT have remarkable mechanical strength, high thermal and chemical stability and wide surface area, and are therefore used for the production of hybrid composite materials [32, 34–36].

A fourth category of NP is cellulose nanomaterials. They are derived from abundant renewable organic biomaterials, and have been attracting much interest because of their high crystallinity, chemical versatility, low density and renewable 'green' nature [2, 3, 37], and in particular for the fabrication of hybrid G-nanocellulose nanocomposite [38–40].

The last category of nanoparticles depicts nanoclays (NC). These are some of the most abundant nanosized materials, normally available in hundreds of tons and broadly used in different applications [41]. NC are organically modified layered silicates with applications as a reinforcement filler in hybrid nanocomposite [12, 42]. In the preparation of hybrid nanocomposites, many NC (montmorillonite, kaolin, halloysite and bentonite) along with silica and GO nanoparticles are used.

In this chapter, key findings of the characterization techniques for hybrid nanocomposites, whereby G and NP are distributed into a matrix, are reviewed. This chapter also explains that the synthesis of these nanocomposites varies depending on the nanofillers' properties; i.e., the G and NP, its dispersion and alignment as reinforcements within the polymer matrix, as well as the interaction of the polymer matrix with the reinforcement. Examples of morphology, structure and property, including the relationship between structure and property, are explored upon characterization. This perspective on the properties of G-NP hybrid materials will provide a detailed view of the current stage of characterization techniques, highlighting the obstacles and new directions for the future production of G-NP hybrid materials.

2 Hybrid Nanocomposite Based on Graphene and Nanoparticles as Advanced Materials

2.1 Graphene and Nanoparticles as Hybrid Nanomaterials

2.1.1 Graphene-Metal and Metal Oxide

G and its derivatives could be obtained by following a top-down (mechanical cleavage or liquid phase exfoliation) or a bottom-up (such as chemical vapor deposition, arc-discharge, chemical conversion, unzipping carbon nanotubes, and epitaxial growth on SiC) preparation method [43].

G-metal and metal oxide hybrids have excellent properties, with promising applications in electronics, sensors, solar cells, batteries, and supercapacitors [11, 19, 20]. Their synthesis could be achieved by using various preparation methods based on microwave-assisted synthesis, thermal evaporation, chemical reduction, photochemical synthesis and electroless metallization [13, 44, 45].

In the case of metals, nanoparticles precursors, *i.e.* metal salts, are generally reduced in a solvent containing GO and rGO [47]. Due to the weak van der Walls interactions, these graphene derivatives tend then to aggregate and even stack to form graphite in the solution [47]. Hence, by attaching metal NP, it is, in fact, possible to prepare individual G sheets and to reduce their agglomeration [47]. In many instances, researchers use this direct chemical reduction approach in order to prepare a large variety of G-metal nanohybrids by combining metal precursors with G or its derivatives, GO and rGO [20, 22, 48]. Among the many deposition approaches of G-NP fillers onto polymers, G and metal hybrid nanostructures are some of the most effective platforms for various applications [9, 45, 49]. For instance, in order to obtain a homogeneous suspension of exfoliated GO, Feng et al. prepared G-TiO_2 by dispersing GO in an ethanol solution under ultrasonication and by adding then $Ti(OPr)_4$ [46]. The resulting solution was then moved to an autoclave and placed in the oven for 12 h at 150 °C [46]. The desired product was thus isolated by centrifugation, thoroughly rinsed with deionized water and ethanol prior to be vacuum-dried [46]. The development procedure as shown in Fig. 1 resulted in a G-TiO_2 hybrid in the form of black, gray powder [46]. The G-TiO_2 hybrids (2 wt%) was used as filler for PVC films, with a glass transition temperature that increased by 3.5 °C and a storage modulus that increased by 50% relative to a pure PVC film [46].

2.1.2 Graphene-Metal Alloy

Owing to the great synergetic performance and long-term working stability of hybrids, the G hybridization with nanometal alloys has shown high potential for various applications [25, 50]. Synthetic methods have integrated various metal alloys on the G surface to reach a perfect control of their morphological and structural properties, by enhancing the adhesion and by limiting the possibility of their dissolution

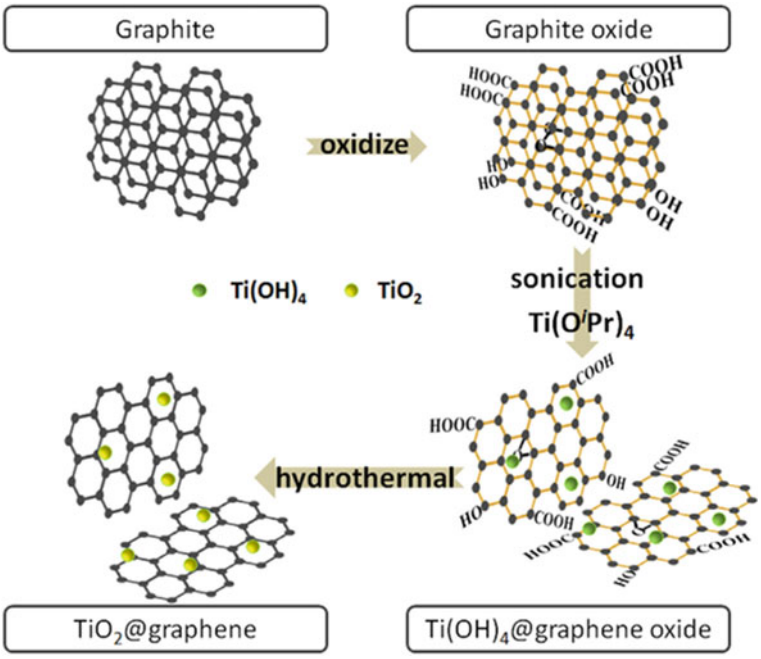

Fig. 1 G-TiO_2 hybrid preparation and structure schematic presentation [46]

and aggregation [22, 28, 50]. To date, numerous novel metal alloy nanostructures integrated on G nanosheets have been widely produced simply by changing the conditions of the reaction, such as the concentration of the precursor, the temperature of the reaction and introduction of the dispersion agent. The nanohybrids obtained displayed very interesting morphologies that were compatible with unique chemical and physical properties [25, 27, 28]. For example, in order to produce G-nanoalloy (Palladium-Copper) hybrid, precursors (Na_2PdCl_4 and $CuSO_4$ of molar ratio 1:3) were mixed together with a suspension containing G. As shown in in Fig. 2, during this preparation method, metal ions from precursors such as $PdCl_4^{2-}$ and Cu^{2+} were adsorbed onto the surface of G nanosheet thanks to a coordination effect between its remaining oxygen moieties and each ion [28].

2.1.3 Graphene-Carbon Nanotubes

In recent years, carbon-based nanofillers such as G and carbon nanotubes (CNT) in nanocomposites have been shown to have better structure and functional properties and a broad range of applications [51, 52]. CNT are prepared using various process techniques including chemical vapor deposition, laser ablation, arc evaporation, electrolysis, flame synthesis, etc. [53, 54]. The CNT are generally used as a filler due to their excellent filler properties including a high conductivity and a superior aspect

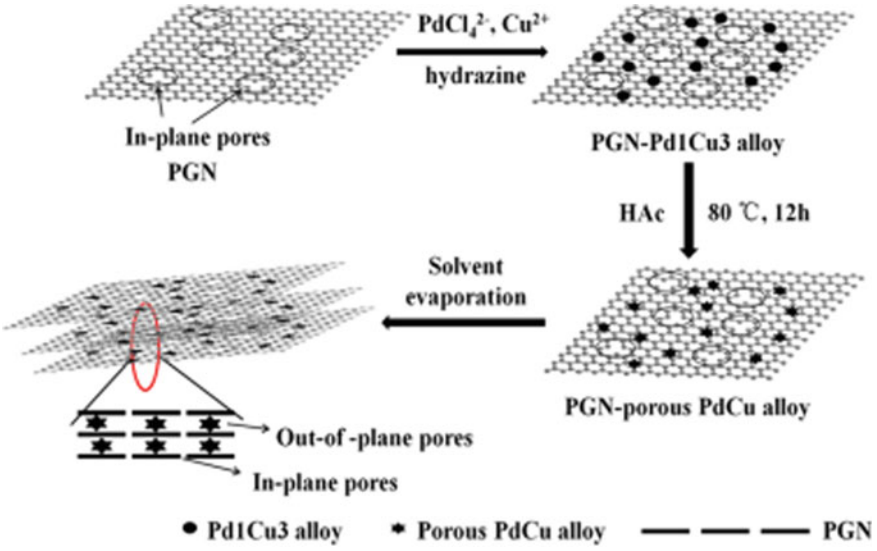

Fig. 2 Hybrid processing design of 3D G-nano alloy (G-PdCu) [28]

ratio and tensile strength. G fillers have also the potential to adjust or fine-tune the properties of targeted materials, which attracted various interests of several scientists working in different research fields [55–57]. Furthermore, a homogenous dispersion could be achieved during the early stages of processing of nanocomposites by incorporating CNT into the polymeric matrix limiting in fact their aggregation [30, 58]. For this reason, several research groups reported on the successful preparation and utilization of G-CNT hybrid fillers in diverse applications such as energy storage, sensing, water treatment, capacitors, etc. [34, 59–61].

The characteristics of G, CNT or hybrid fillers depend upon many parameters such as the type of CNT, the type of G, the purity, the size of CNT, the aspect ratio of the nanotubes, the loading, the interactions, the alignment, and the anti-agglomeration of G and CNT [63]. Three techniques are used for processing G-CNT hybrids: solution mixing, chemical vapor deposition and in situ polymerization [64–66]. In a study by Kong et al., a two-stage method for G-CNT hybrid synthesis was developed. This is shown in Fig. 3 [62], where it was reported that the CNT growth uniformly on the G surface followed that of the modification agent, resulting in the creation of a complex interface driven by a covalent C–C bonding connection between the G and CNT [62]. Similar observations were made by various studies on G-CNT hybrid [67–69].

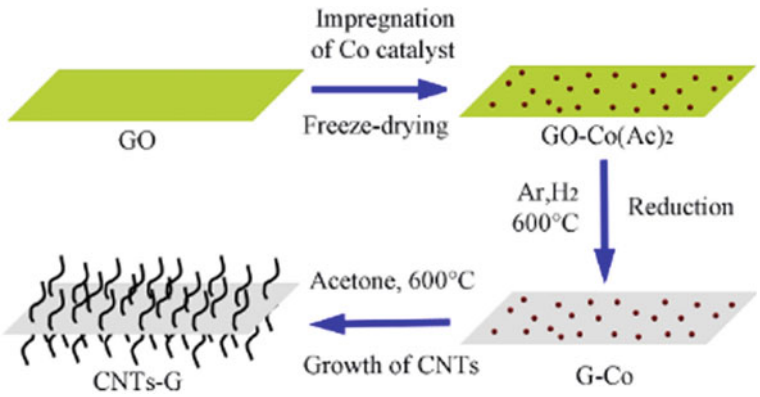

Fig. 3 Schematic diagram of the G-CNT hybrid synthetic method [62]

2.1.4 Graphene-Nanocelluloses

Nanocellulose, an organic compound extracted from natural resources, is biodegradable, biocompatible, and can demonstrate interesting properties when used as a filler in composites [70, 71]. Nanocellulose has unique characteristics including a large aspect ratio, good mechanical properties, good flexibility and hydrophilicity, explaining why it is therefore used as a filler to form nanocomposite [72]. The hierarchical structure and the presence of rigid chains on its molecular structure allow the formation of composite containing nanocellulose with flexible substrates and other materials [73]. Nanocellulose is found in the form of crystals (CNC) or fibrils (CNF), which can be dispersed and self-assembled easily in a solution under the ultrasonication process [72, 74]. Graphene, on the other hand, is a two-dimensional carbon nanostructure that has drawn considerable attention in the development of composites because of its excellent thermal properties, large surface area, high strength and young's modulus [75]. However, due to the presence of strong intermolecular π-π stacking attraction forces and van der Waals interaction, G has the tendency to aggregate irreversibly even in water or in organic solutions [75].

Researchers have suggested a new strategy to hybridize G with amphipathic nanocellulose during GO reduction, acting as a stabilizer or a supporting agent [15, 38, 40]. Depending on the G-nanocellulose ratio, the resulting hybrid material is made up of G layers surrounded by nanocellulose to a greater or lesser limit [76]. The G-nanocellulose hybrid was demonstrated to have a covalent chemical structure and an excellent aqueous suspension stability, which greatly facilitated G dispersion [77]. Studies have reported that the abundance of oxygen-containing groups decorated with G can combine with nanocellulose hydroxyl groups and oxygen atoms, which are advantageous for the homogeneous dispersion of G and nanocellulose in the shaped hybrid nanofiller [40, 76, 78]. Hence, the preparation of covalent cross-linked G-nanocellulose hybrids was realized by esterification between hydroxyl groups [79].

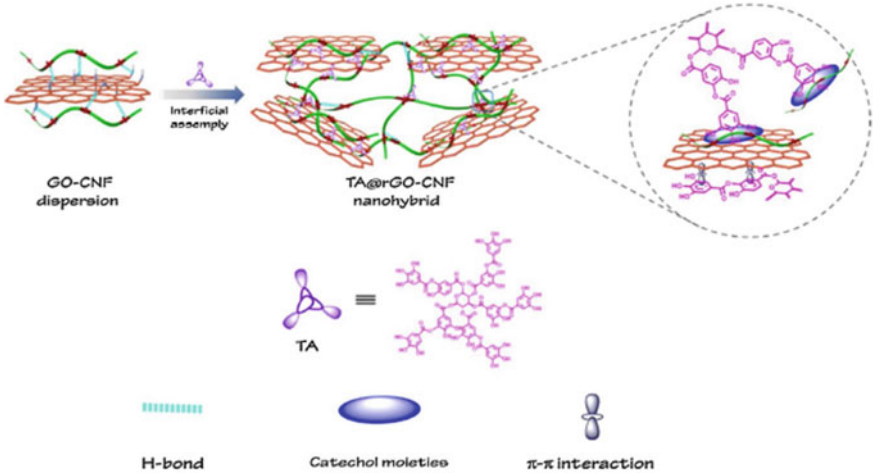

Fig. 4 Schematic diagram and nanohybrid structure of rGO-CNF [76]

Montes et al. prepared fillers based on G-CNC by assisting the graphite exfoliation in a liquid-phase containing CNC. By following this novel approach, graphene flakes seem to be stabilized in aqueous dispersions [80]. Similarly, as shown in Fig. 4, Wang et al. produced rGO-CNF hybrid with rGO and CNF aqueous suspension by using a one-step synthesis combining a chemical reduction and an induced materials assembly, which was facilitated by the addition of the tannic acid [76]. Due to the functional catechol chemistry of tannic acid, the interfacial interactions between rGO nanosheets and CNF (which includes π-π and hydrogen bonding) improved; this created a strong adherent coating acting as a capping layer to stabilize and decorate the obtained rGO-CNF hybrid [76].

2.1.5 Graphene-Nanoclays

Natural occurring nanoclays (NC) like montmorillonite, bentonite, laponite, halloysite and kaolin were used as nanofillers for the production of composites in a variety of industrial applications [81]. The NC platelet structure allows it to form a protective barrier once a high degree of exfoliation with a good dispersion has been achieved, resulting in an improved mechanical performance of materials [82]. Similarly, G is a member of the family of monolayer carbon atoms, fully compacted into a 2D honeycomb network, which acts as a fundamental structural block for graphite-based materials [83–86]. A high-performance material is thus obtained by producing, a hybrid composed of GO and NC [82, 83, 86].

In different studies, GO hybrids reduced by halloysite nanotubes were prepared by simultaneous reduction and hybridization of GO with halloysite nanotubes [84, 87, 88]. It was observed that the hybrids had a perfect coverage structure and that the

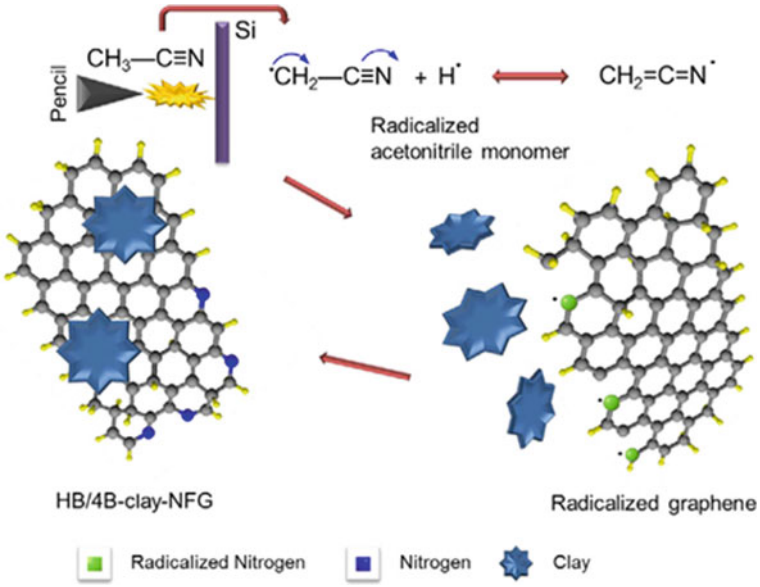

Fig. 5 Proposed framework for G-NC hybrid formation [90]

intercalation of halloysite nanotubes within the GO sheet interlayers was likely due to the excellent compatibility between G and halloysite nanotubes [87]. Research on GO-montmorillonite hybrid has shown that the hybrid material's d-spacing is observed between that of the GO-montmorillonite and the structure of the GO flake-pillared montmorillonite [89].

NC's role in the manufacture of G-based hybrids was thus explored due to its high chemical stability, specific swelling capability and ability to exchange ions [41]. As seen in the Fig. 5, the scattered nanoclay particles are physically or chemically absorbed at the ionized sites of the G layers in the hybrid [90]. The particles of NC do not attract or interact with the sites of radicalized G as they are effectively surrounded by the radicals of hydrogen [90]. The distributed radicalized G has a high affinity with H and CH2-CN radicals and generates, as a result, G-NC hybrid pyridinic and pyrrolic systems [90].

2.2 *Hybrid Nanocomposites Based on Graphene and Nanoparticles*

2.2.1 Hybrid Polymer Nanocomposites Based on Graphene and Metal/metal Oxide

Hybrid G-nanometal polymer composite materials is a subject that gained much attention recently [6, 91, 92]. In particular the design and preparation methods of polymer nanocomposites reinforced by G-nanometal have become common practice, since these hybrid fillers provide unique properties to the polymer matrix [92, 93]. The hybrid G-nanometal/metal oxide in the polymer matrix has the advantage that the G sheets serve as a loader for regulated metal NP production and can prevent the self-assembly of small metal NP during the preparation of the composite nanomaterials [6, 18, 94]. Metal oxides play here a significant role in improving the polymer's immobilization and thus the enzyme stability [95].

For instance, the polyvinyl chloride (PVC's) glass transition temperature reinforced with G-TiO_2 hybrid increased from 71.3 to 74.8 °C compared with neat PVC, indicating that the segmental chain mobility is limited by the intense interfacial interactions between the nanohybrids and the polymer matrix [46]. Kumar et al. prepared a multifunctional biodegradable material where hybrid graphene-silver (rGO-Ag) nanoparticles were used to enhance poly-caprolactone (PCL) matrix, as demonstrated in Fig. 6 [6]. Comparing with rGO or Ag nanoparticles alone, rGO-Ag hybrid nanoparticles were found to be well dispersed in the polymer matrix due to enhanced exfoliation [6]. In addition, it was noted that uniformly scattered rGO-Ag hybrid nanoparticles resulted in a 77% increase in the PCL Youngs' modulus at 5 wt% filler, which exceeded significantly the improvements achieved with the addition

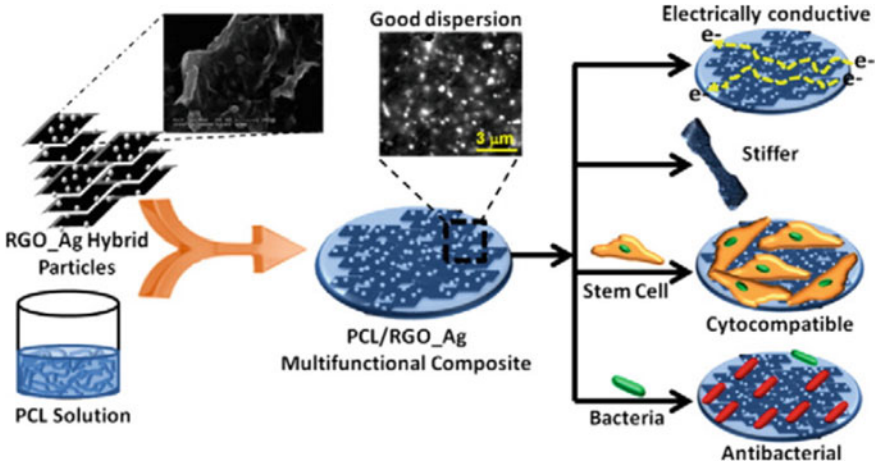

Fig. 6 Schema polymer nanocomposite incorporated with rGO-Ag hybrid [6]

of rGO or Ag nanoparticles alone in the PCL [6]. Other improved properties include conductivity, stiffness, antibacterial property and cytocompatibility [6]. Likewise, by adding 0.25 phr rGO—Fe_2O_3 in the epoxy matrix, tensile strength, flexural strength and impact strength improved by 56%, 81% and 112% respectively [92].

2.2.2 Hybrid Polymer Nanocomposites Based on Graphene and Metal Alloy

Metals' scarcity, mass interaction and stability have become the critical limiting factors that hinder the commercial applications of metal-based materials, in recent years [96, 97]. A number of strategies have been adapted to enhance those properties, two of which are: i. reducing the size of metals to a nanoscale, which can provide more active sites and increases the use of metals per mass, ii. alloying with earth-abundant transition metals (Cu, Zn, Ni, and Fe), which may improve the metal-based hybrid's mass activity and stability due to the synergetic effects resulting from changes in the nano-alloy surface physical and chemical natures [26]. These approaches and others have helped the rapid advancement of G-based nanocomposites, highlighting the nanometal alloys strong mechanical reinforcement strength, large specific surface area, excellent biocompatibility and good thermal properties [48, 98, 99].

Hong et al. prepared poly(methyl methacrylate) (PMMA) nanocomposite as shown in Fig. 7, reinforced by rGO-NiAl hybrid, using a simple solution blending method, in order to investigate its effect on increasing the composite's thermal stability [48]. It was observed in the thermal studies that a greater residue of 3.7 wt% was obtained, which was attributable to the combination of the physical barrier effect of rGO and the NiAl alloy nanoparticles, hence confirming enhanced thermal stability of the PMMA hybrid nanocomposite [48]. Physical characterization demonstrated that poly (triazine imide) (PTI) nanosheets hindered G nanosheets restacking and allowed the even-scattering of the 2.5 nm PtSn alloy nanoparticles on the PTI graphene support materials [99].

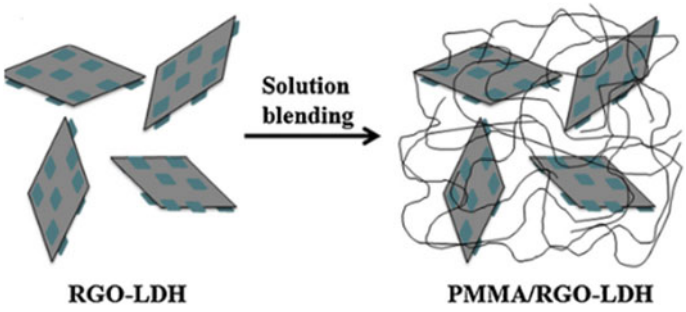

Fig. 7 Schema of the formation of poly(methyl methacrylate) composite reinforced with rGO/NiAl-layered double hydroxide hybrid (presented as rGO-LDH) [48]

2.2.3 Hybrid Polymer Nanocomposites Based on Graphene and Carbon Nanotubes

The improvement of the nanocomposite materials properties could be achieved by using CNT as fillers since the CNT have a high Young's modulus, a high tensile strength, a high aspect ratio, a low density, etc. [29, 100]. These exceptional properties make CNT ideal as a reinforcement additive in hybrid nanocomposites. On the other side, G and its derivatives can be used to modify the inherent properties or induce new properties to the matrix [101, 102]. G based-polymer composites show improved mechanical, thermal, and barrier properties compared to the neat polymeric materials [103]. However, difficulties lie in transforming or imparting the unique properties of G or CNT alone to the polymer [104, 105]. The homogeneous dispersion of the filler in the matrix is crucial in ensuring a good interfacial interaction and adhesion between the phases [106].

The incorporation of the G-CNT hybrid filler to the polymer matrix has more attractive properties compared to the neat polymer [108]. Hybrid polymer nanocomposite based on G and CNT can be used for diverse applications like conduction, coating and films, electromagnetic interference shielding materials for electronic devices, thermal interface materials, etc. [35, 36, 64]. As an illustration, Liu et al. prepared hybrid polyethylene polymer composites based on graphene and carbon nanotubes [109]. They demonstrated an impressive synergetic effect between the G and CNT leading to a clear improvement of the interfacial mechanical properties of the polyethylene matrix [109]. Furthermore, they showed that the reinforcement effect on the covalent bond of the G-CNT hybrid is directly related to the CNT length and radius, and also to the choice of CNT as the use of multi-walled CNT seems to lead to more efficient materials than those made using single-walled CNT [109]. By the addition of GO-CNT hybrid charges to the polymer matrix, it was observed that the composite's storage modulus was the main thermal response speed factor [63]. This observation could be attributed by the presence of specific molecular interactions occurring within the G-CNT hybrid and the polymeric structure.

In another study, Bagotia et al. successfully prepared polycarbonate/ethylene methyl acrylate nanocomposites by following a melt-blending method using different ratios of the G-CNT hybrid filler, as shown in Fig. 8 [107]. Among the tested materials, hybrid filler composites with 10 phr loading (G:CNT ratio 1:3) have a highest tensile strength and tensile modulus than G or CNT based composites at the same loading [107]. In summary, the G-CNT hybrid nanostructure exhibited a synergistic effect improving thus the structural, mechanical and thermal properties of the composite even by selecting a large variety of polymeric matrix, like, exemplified using the poly(vinylidene fluoride) [67], epoxy [63], poly(methyl methacrylate) [110], poly(ether sulfone) [32], poly(vinyl alcohol) [69, 111], poly(dimethylsiloxane) [62], poly(ether-ether-ketone) [112], poly(styrene-b-butadiene-b-styrene) [112], etc.

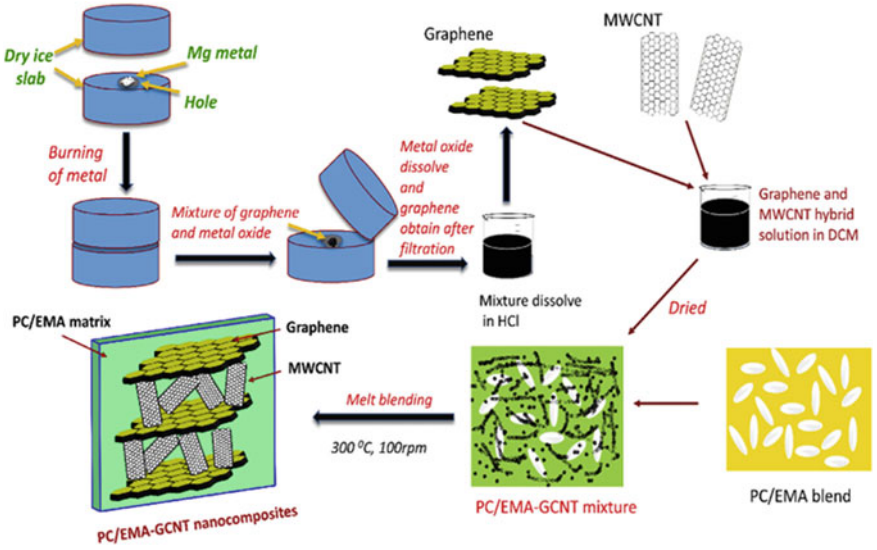

Fig. 8 Graphical description for manufacturing of G-CNT hybrid reinforced polymer composite [107]

2.2.4 Hybrid Polymer Nanocomposites Based on Graphene and Nanocelluloses

Nanocellulose (CNC or CNF) was used individually as an efficient reinforcing fillers on many kinds of polymers [73, 113]. Driven by unique properties (high specific strength, biocompatibility, biodegradability, low weight, abundance, barrier properties and capacity for reinforcement) nanocellulose is recognized as an ideal candidate for the development of polymer nanocomposites [71, 114]. On the other hand, G and its derivatives are also well-known to be potentially the best options leading to high enhancement of polymeric nanomaterials due to their favorable scalability, high mechanical/thermal conductivity, and chemical flexibility [103]. However, as with most nanocomposites, several crucial challenges, such as incomplete G exfoliation, uneven dispersion of fillers, high hydrophilicity of nanocellulose and weak G-matrix adhesion, present limited the full functionality of most described nanomaterials containing G or nanocellulose alone [78, 103, 115].

The development of sustainable and biodegradable nanocellulose aligns with an environmentally friendly approach to mediate G dispersion in aqueous media and its integrated morphology in polymeric matrices such as polyvinyl alcohol [15, 79, 80], polyethylene [40], poly-lactic [38, 78], polyphenol [76], rubber [77], etc. Recent studies have therefore explored the use of sustainable carbohydrate polymers (i.e. cellulose), as they are biocompatible and environmentally friendly, thus achieving

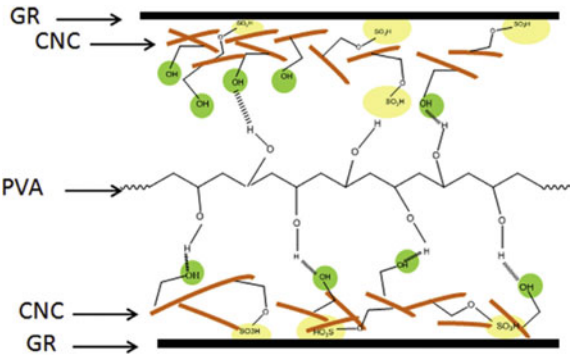

Fig. 9 Schematic presentation of poly (vinyl alcohol) nanocomposites with G-CNC hybrid [80]

the functionalized biopolymer G-nanocellulose hybrids to reinforce the nanocomposites [40]. The obtained G-nanocellulose hybrids have excellent aqueous suspension stability, which greatly facilitated their dispersion into polymer matrix [15].

In many cases, it was noted that the G-cellulose nanohybrids are selectively located in the interfaces between the polymer microspheres and are assembled into a 3D hierarchical conductive network structure during co-coagulation [77, 79, 116]. Interestingly, the use of G-nanocellulose hybrid was considered a simple approach not only to prevent the use of chemicals modifying agents, but also to enhance the conductivity and mechanical properties of G-based composites prepared with randomly scattered G, through traditional production procedures [39, 77, 79].

For instance, the G-CNC hybrid was combined with poly(vinyl alcohol) (PVA) aqueous solutions to prepare PVA-based nanocomposites (PVA/G-CNC), using a simple and environmentally friendly casting process [80]. It was stated that the synergistic reinforcing effect of G-CNC was obtained through the presence of strong H-bonds between -OH groups of the PVA and CNC enhancing thus their interfacial interaction. This was also achieved thanks to the presence of CNG, promoting the dispersion of graphene in the PVA matrix, as shown in Fig. 9 [80]. Similarly, owing to the synergistic reinforcement of G-CNC, it was noticed that Young's modulus, tensile strength and resilience of the PVA nanocomposite containing 5 wt% hybrid nanofiller (G:CNC ratio 1:2) increased substantially by 320%, 124% and 159% respectively; and the break elongation remained substantial compared to the pure PVA matrix [15].

2.2.5 Hybrid Polymer Nanocomposites Based on Graphene and Nanoclays

Nanocomposites made of clay-based polymers have gained significant interest from the scientific community over the past decade [81]. Researchers studied particularly the potential for reinforcement of polymeric matrix with modified nanoclays (montmorillonite, bentonite, laponite, halloysite and kaolin), so as to improve its properties such as thermal, barrier, mechanical and resistance to flammability [84, 117, 118]. Compatibilizers such as G are also used in the preparation of nanocomposites as well

as modifying the nanoclays (NC) to enhance the dispersion of the filler particles [86]. Hence, the synergetic effect of dispersion and flame retardancy was the key element to the introduction of G-NC hybrid fillers in the polymer matrix [119].

In addition to flame retardants, G-NC hybrids have been used in various polymer matrices for various other applications such as nylon thermomechanical properties enhancement [82], supercapacitors electrode materials [41, 85], superabsorbent [88], water treatment [84, 118], thermoplastics manufacture [120], etc.

Figure 10 shows graphene oxide-halloysite nanotubes hybrids (HRGO) prepared by simultaneous reduction and hybridization of GO with halloysite nanotubes. The HRGO have been integrated into an epoxy matrix to improve its thermal and the mechanical properties [87]. In fact, the Halloysite nanotubes effectively impeded the accumulation of GO sheets in the epoxy matrix [87]. Similarly, the epoxy nanocomposites showed improvements of 36, 16, 27 and 19% in Young's modulus, tensile power, critical stress intensity factor (KIC) and critical energy release rate (GIC) were achieved using GO-attapulgite hybrids, respectively [121]. In a different study where hybrids with different montmorillonite/GO ratios were examined, the 5:1 mass-ratio hybrid offered better dispersibility and more effectively, while the mechanical strength of epoxy-based composites was enhanced [89].

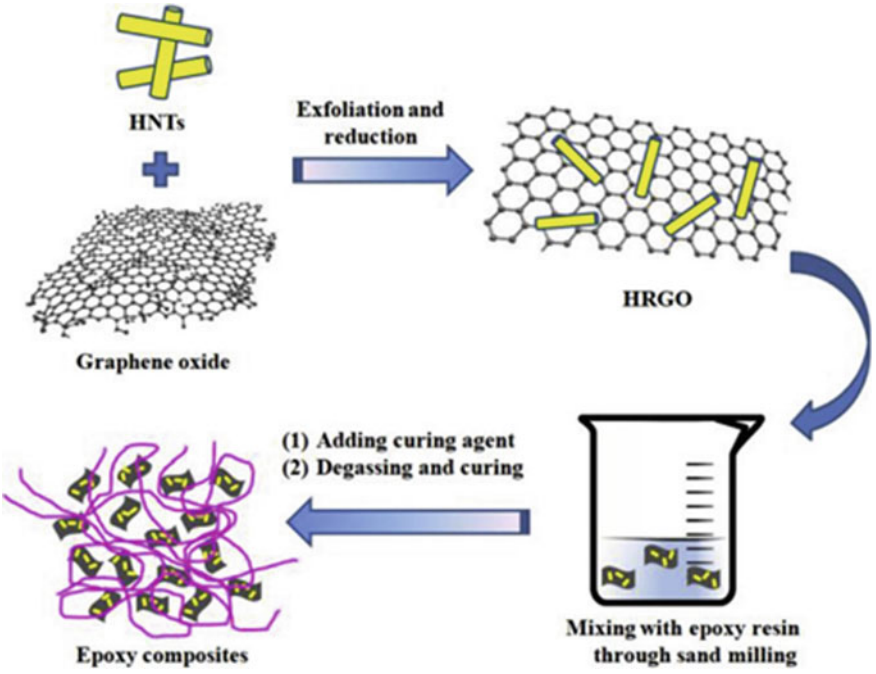

Fig. 10 Schematic overview of GO-halloysite nanotubes hybrid (HRGO) preparations and HRGO-reinforced epoxy composites [87]

3 Characterization Techniques

In materials science, material properties are fundamentally linked to microstructure, which necessitates knowledge of the recent characterization approaches [122, 123]. This is because materials such as thermoplastics, composites and hybrid films have several elementary constituents dispersed in more than one process of fabrication. Characterization is, otherwise, essential for the systematic production of these different materials and for determining their functionality in practical uses. Several commercially available techniques are used to study materials, e.g., microscopy, spectroscopy, and thermal analysis. Each of these techniques is typically used for a define type of materials or for the retrieval specific information. This presents a technical challenge in choosing the adequate characterization technique when dealing with a specific sample. Researchers or engineers must therefore specify which information is required to thoroughly describe each substance and use that data to understand its behavior, create new and advanced materials, minimize costs, or comply with regulatory standards. The following sub-chapter provides all the contexts required to understand the, as characterization technologies of graphene-based nanohybrid and its composite materials, with particular attention to the current and most commonly used techniques as presented in Fig. 11.

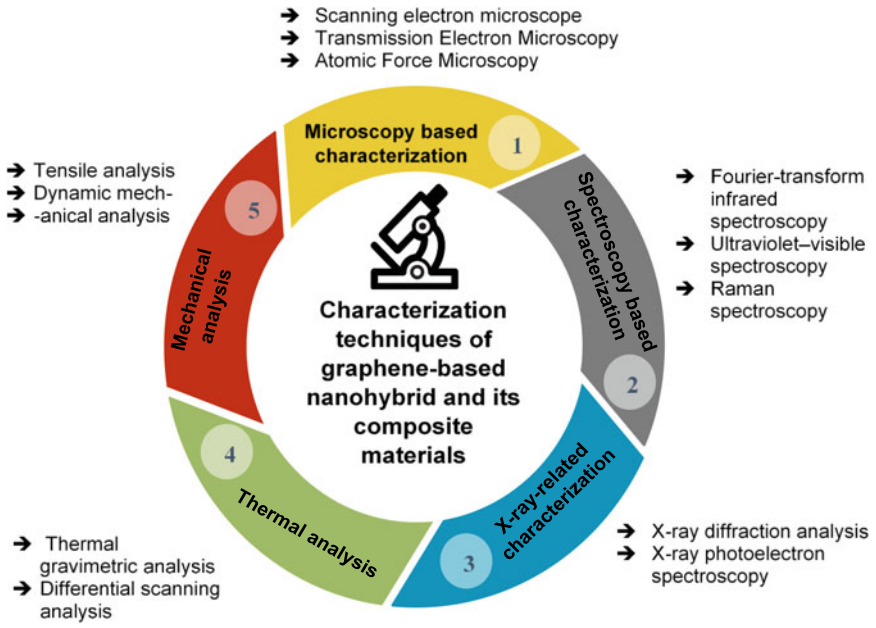

Fig. 11 Categories of the characterization techniques used to study G-NP based hybrid composites

3.1 Microscopy-Based Characterization

3.1.1 Scanning Electron Microscope, SEM

Roughness, morphology, size and state of dispersion of particles in a material can be measured using several microscopy techniques at various length scales. Scanning electron microscopy (SEM), transmission electron microscopy (TEM) and atomic force microscopy (AFM) can provide a straightforward way of observing and analyzing the dispersion of particles at various lengths qualitatively [124]. SEM used a focused electron beam to scan a surface and subsequently present an image [125]. SEM has been used in several works in order to study the dispersion of the graphene-based hybrid nanofillers and examine the surfaces of their composites [23, 32, 45, 80, 126].

With the help of SEM images it was possible to confirm that SnO_2 nanocrystals are attached to the surface of rGO sheets, where the presence of SnO_2 nanocrystals proved that GO and $SnCl_4$ hydrothermal treatment is an effective preparation method of the rGO-SnO_2 hybrid [127]. Similarly, the GO-TiO_2 hybrid SEM images proved that dense TiO_2 nanocrystals were tightly attached to GO sheets and did not separate under sonication [128]. Furthermore, from the analysis of the SEM images of the GO-TiO_2 hybrid, it was possible to conclude that the coating of TiO_2 nanocrystals on graphene is denser with increasing the Ti $(BuO)_4$/GO feed ratio [128]. Further analysis of the dispersion of nanoparticles in the hybrids shows that the SEM images (Fig. 12a) exhibit the presence of individually large Cu or copper oxide particles in the hybrid rGO-Cu (ratio: 1–2) [21]. The rGO-Cu hybrid SEM image (ratio: 1–1) shown in Fig. 12b also clearly indicates the size of the non-uniform nanoparticles in the hybrid [21]. An increase of the mass ratio of rGO-Cu to 2:1 leads to highly dispersed metallic Cu nanoparticles with a small size distribution of 50–100 nm within the GO structure, as shown by SEM image in Fig. 12c. Further increase of the mass ratio of GO-Cu to 5:1 leads to even smaller Cu nanoparticles on the surface of rGO nanosheets with a size distribution of 5–15 nm, as shown in Fig. 12d [21].

SEM analysis was also used to investigate the fracture surfaces of epoxy composites reinforced with G-CNT nanofillers [106]. For the composite with the G-CNT hybrid filler structure, the dispersion of the CNT within the matrix is improved with no rich CNT domains on the surface [106]. The analysis showed that a small amount of G has greatly modified the dispersion and state of aggregation of CNT. In fact, there were no voids or gaps found on the surface of the fracture [106]. Yang et al. demonstrated that the SEM images demonstrated a better dispersion and homogeneity of G and CNT within the epoxy matrix for composites which contain the G-CNT hybrid nanofillers [126]. The SEM images proved that adding CNT significantly affected the dispersion of graphene and the state of aggregation in the epoxy matrix [126], and confirmed the impact that the synergetic effects that CNT and G have on the mechanical properties and composite thermal conductivity [126].

The SEM images (Fig. 13) of the cryogenically broken cross-section of the nanocomposite films obtained in the polyimide (PI) matrix brings to light details

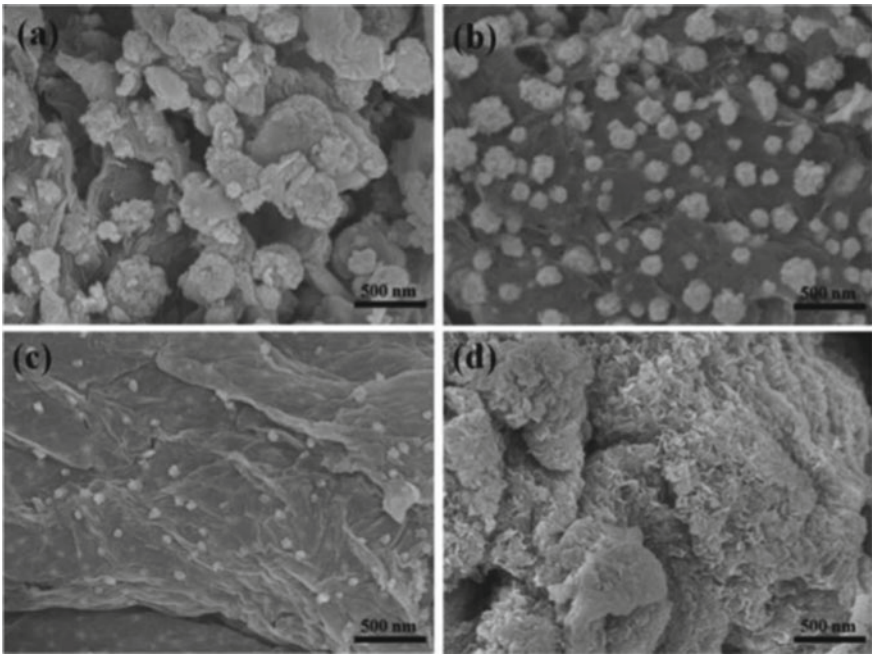

Fig. 12 SEM images of rGO-Cu hybrid at different ratios [21]

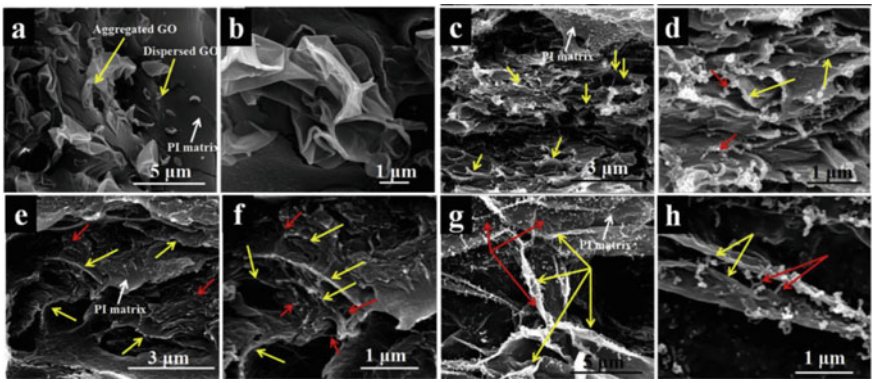

Fig. 13 SEM observations of hybrid polyimide (PI) polymer nanocomposites based on GO-CNT fillers [129]. The yellow arrows indicate the GO nanosheets and the red arrows indicate the CNT

of these nanofillers [129]. For example, many of the GO nanosheets were aggregated together in the PI/GO nanocomposites (Fig. 13a), aside from some scattered GO nanosheets. In addition, the zone magnified in Fig. 13b suggests that the GO nanosheets were poorly compatible with the PI matrix and formed an extreme aggregation, resulting from the wide surface area of GO, which easily stacks to

form agglomerates [129]. The GO agglomeration decreases the area of interaction between GO and PI, leading to low-efficiency GO-reinforcing. Figure 13c, d show the PI nanocomposites packed with the GO-CNT hybrid. It is seen that the introduction of CNT prevents the aggregation of nanosheets of GO and increases the area of interaction between matrix GO and PI. For PI nanocomposites filled with the GO-CNT hybrid (shown in Fig. 13e, f), GO is firmly embedded in the PI matrix, which suggests an excellent stability of hybrid GO-CNT nanofillers in the PI matrix, due to the creation of hybrid nanostructure bound by the hydrogen bond interaction [129]. Additionally, 3D hybrid networks were formed between GO and CNT and well distributed in the PI matrix containing GO-crosslinked and oxidized CNT nanofillers (Fig. 13g, h), which is regarded to be of great advantage in increasing the performance of PI matrix [129].

3.1.2 Transmission Electron Microscopy, TEM

Besides SEM analysis, TEM is a technique that also uses an electron beam to image a sample, offering a much better resolution than light- imaging techniques [130]. TEM is the best tool for calculating the scale of the NP, the grain scale, the size distribution and the morphology of hybrid nanofillers [129]. For example, analysis of the TEM images allows the confirmation of the morphology structure of nanohybrid based on exfoliated G and CNF [131]. Using a TEM image of the G-CNF hybrid, it was observed that graphene had a crumpled geometry and that CNF were found on the G surface [131]. The selected area electron diffraction pattern (SAED) from the TEM analysis showed that standard six-fold symmetry diffraction spots with the outer hexagon spots appear slightly weaker than those of the inner hexagon, which also confirms the obtained monolayer graphene, as shown in Fig. 14.

TEM images were also used by Taj et al. to confirm the existence of gold nanostructures on the 2D layer of a G hybrid [132]. The images demonstrated that it is possible to obtain a uniform distribution of gold nanostructures (2–8 nm diameters) anchored on nanosheets of G by in-situ synthesis [132]. Besides, the corrugated structure of the

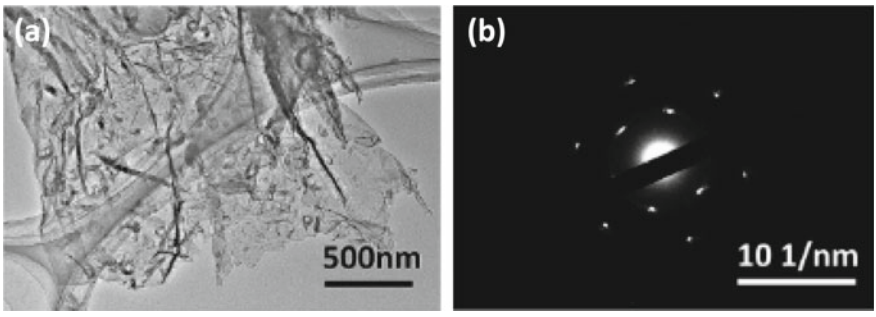

Fig. 14 **a** TEM images and **b** SAED pattern of graphene-chitin nanofibers (G-CNF) hybrid nanomaterial [131]

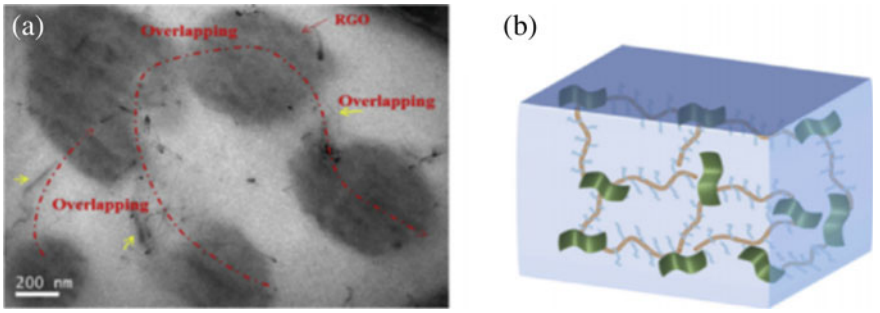

Fig. 15 TEM images of the styrene-butadiene rubber composites containing 3% rGO-CNT. **a** The red lines illustrate the pathways of heat transfer. **b** Schematic diagram of the proposed thermal conduction [133]

G sheets was possible to demonstrate [132], and it was observed that approximately 75% of the particle size distribution was with a dimension of 2–4 ± 1.2 nm, while the remainder occurs within a range of 4–8 nm [132]. Similarly, typical G-PtAu hybrid TEM images were obtained with various magnifications, showing that PtAu bimetallic nanoparticles with an average diameter of 3.3 nm are spread evenly on G nanosheets [50]. Furthermore, Taj et al. confirmed that the results of microscopy obtained by SEM and TEM are in agreement and define the novel morphology of the hybrid G-NP [132].

Yue et al. analyzed TEM images of microtomed samples at an average filler concentration of 0.1 wt% in order to examine the filler dispersion in the epoxy composites with G-CNT hybrid nanofillers [106]. For the nanohybrid epoxy composite network, the dispersion of the filler significantly increased [106]. The nanoplatelets of 2D graphene were intercalated between the nanotubes of 1D carbon, which could contribute to the creation of a network of 3D fillers, and lead to better mechanical and electrical properties [106].

Through TEM analysis, the rGO-CNT hybrid has shown a good dispersion in the rubber matrix [133]. Song et al. confirmed the introduction of CNT bridges into the isolated rGO nanosheets, which resulted in reduced interfacial thermal resistance from the filler-filler interface and the filler/rubber interface (Fig. 15a) [133]. Thus, the ultimate thermal energy of the rubber composites is transferred to strictly defined 3D channels, as demonstrated with the normal red arrows in the model shown in Fig. 15b.

3.1.3 High-Resolution Transmission Electron Microscopy

In the same way as TEM analysis technique, HRTEM is a developed transmission electron microscope imaging mode that allows direct imagery of the graphene-based nanohybrid material's atomic structure [11, 48, 62, 134]. For instance, Chouhan et al. obtained the high resolution transmission electron microscopy (HRTEM) image of

GO-Laponite nanohybrid, which indicated that the GO and Laponite layers are overlapped with each other [134]. The overlapping is a clear indicator of the interactions between the GO and Laponite layers at nanoscale [134]. The hexagonal sequence of bright spots in the selected region electron diffraction (SAED) pattern, obtained from the HRTEM analysis, showed a bright spot, identifying the group of {1100} plane perpendicular to the basal plane (0001). This indicates clearly the presence of GO sheets. Whereas in the SAED pattern, the amorphous ring pattern suggest the existence of Laponite [134].

Similarly, Fig. 16 displays TEM, HRTEM images of a silica and G-silica nanohybrid, as well as the associated select area electron diffraction (SAED) patterns [135]. It is seen that the size of the silica particles is very uniform (Fig. 16a) [135], and that the silica aerogel sample is primarily composed of amorphous and disordered structures, as disclosed in the HRTEM image in Fig. 16b [135]. Furthermore, the silica aerogel SAED pattern (Fig. 16c) reveals diffraction rings without any diffraction dots, which validates the existence of an amorphous structure of the silica aerogel [135]. Figure 16d shows a TEM image of a G-silica nanohybrid, in which many small-layered graphene layers wrinkled on a silica aerogel can be identified [135]. The HRTEM image of G-silica nanohybrid analysis revealed that thin walls as shown in Fig. 16e, usually consist of just a certain layer of graphene sheets formed from silica aerogel. As further confirmation, selected area electron diffraction (SAED)

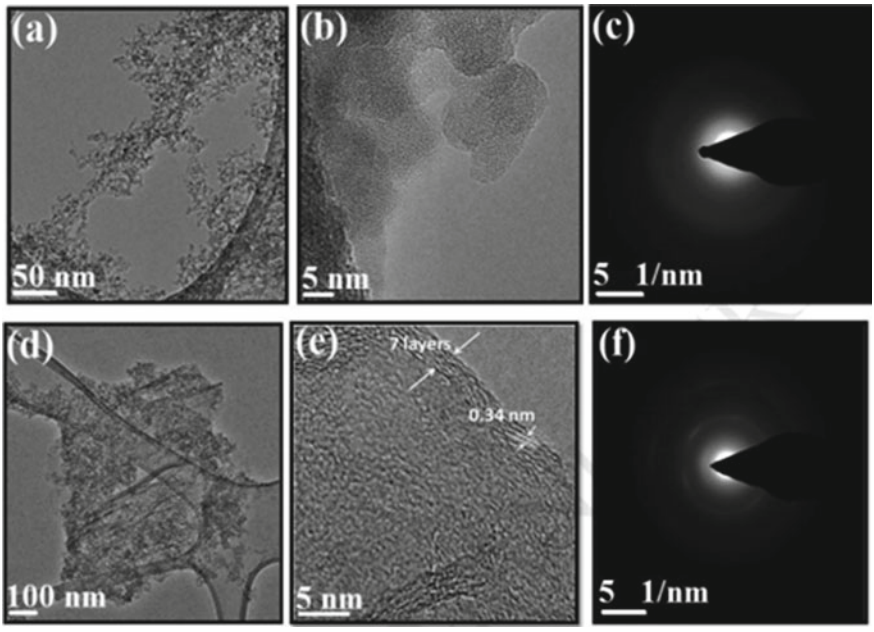

Fig. 16 TEM images of **a** silica, and **d** G-silica hybrids, HRTEM images of **b** silica, and **e** G-silica nanohybrids and equivalent SAED patterns of **c** silica, and **f** G-silica hybrids [135]

was used to uncover the crystal structure of G on silica, as can be seen in Fig. 16f [135].

3.1.4 Atomic Force Microscopy

AFM is another advanced micro-based technology used to analyze a surface in its complete, three-dimensional space, down to the nanometer size [37, 71]. The AFM techniques have been commonly used to study the G-based hybrid filler structure's physical behavior and its effect on a polymer matrix [15, 129, 136, 137]. Illustratively, AFM studies were used to investigate the morphology and measurements of the nanomaterials GO, CNC and their hybrid nanofillers GO-CNC [15]. For CNC, the AFM image demonstrated that there were needle-like nanoparticles for the as-extracted CNC, indicating that their isolation from the treated sugarcane bagasse was productive [15]. On the other hand, the GO's AFM images showed the presence of individual irregularly shaped nanosheets with identical thicknesses and different lateral sizes [15]. AFM characterization of the GO-CNC nanofiller hybrid (GO: CNC-1:2) revealed that the GO surface had become fully and densely covered with randomly arranged CNC [15].

In another study (Fig. 17), the AFM morphology of GO-CNF and rGO-CNF revealed an ultrathin GO surface (~1.0 nm thickness, ~0.6 μm size) [76]. As shown in Fig. 17a, the CNF nanofibers were partially absorbed on the GO surface; the thinness of GO-CNF hybrids was approximately 2.42 nm [76]. In comparison, the thickness of rGO-CNF nanohybrid layer was about 5.245 nm (Fig. 17b), which was much thicker than the GO-CNF specimen [76]. Xiong et al. noted that the AFM images analyses helped realize that the combination of cellulose nanofibers CNF and GO nanosheets resulted in the spontaneous creation of stable 2D hybrid nanostructures with planar GO nanosheets uniformly encapsulated in a dense network of 1D nanofibers [138]. Furthermore, it was also noticed the thick CNF coating

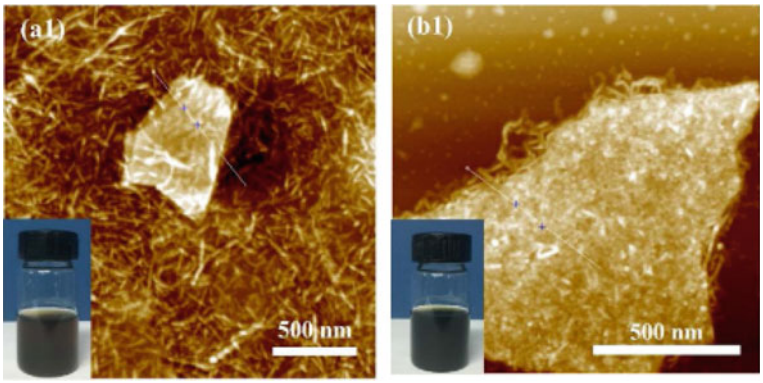

Fig. 17 AFM images of **a** GO-CNF hybrid, and **b** rGO-CNF hybrid [76]

renders them extended from the sides of GO, like long hairs produced around the sides of GO [138].

AFM was also utilized to investigate the surface morphology of the polyimide reinforced with hybrid GO-CNT [129]. It was noted that the surface roughness of the polyimide matrix increased considerably with the addition of either GO or CNT compared to that of pure PI [129]. Compared to all other polyimide-based nanocomposites, the surface roughness value decreased when incorporating the hybrid GO-CNT, and almost identical to that of neat polyimide [129].

For further illustration, Fig. 18 portrays AFM 3D topography images of pure polysulfone (PSf) and composite membranes filled with CNT, rGO and rGO-CNT nanofiller hybrids [136]. The pure PSf film micrograph was found to be coarser with a roughness of 19.89 nm, which showed that an amorphous network is built on the surface [136], While the PSf reinforced with the CNT film exhibited a roughness of 18.12 nm, it addressed improved compatibility of CNT within the PSf matrix. This is illustrated in the topographic image, which shows homogeneously scattered bright patches on the surface [136]. The PSf-rGO film micrograph showed, on the other hand, the presence of a thicker area with a layered and firmer structure, with a roughness of 21.5 nm [136]. The hybrid composite film AFM micrograph showed the presence of several convex hills and walls on the surface with a roughness of

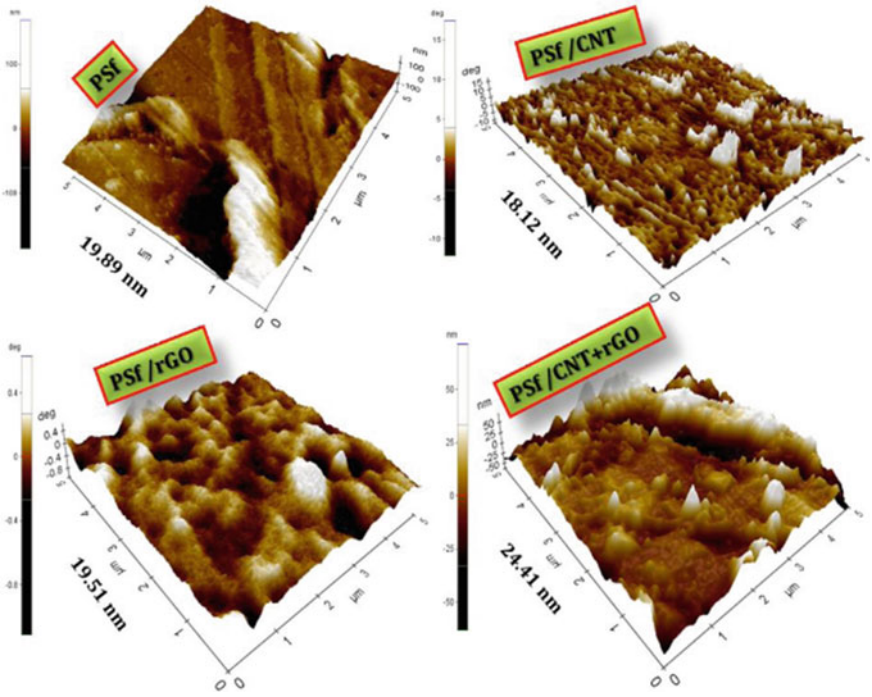

Fig. 18 AFM 3D composite samples topographical micrographs [136]

22.86 nm, which is higher than for the matrix reinforced with G and CNT alone [136].

3.2 Spectroscopy-Based Characterization

Spectroscopy characterization is the study of the interaction between material and electromagnetic radiation by means of electron and atomic energy [139–142]. Many such interactions include spectroscopy of absorption, elastic, resonance, emission and inelastic scattering [143–145]. Spectroscopic studies were essential to the development of nanohybrids and composites based on G [15, 46, 80]. There are several types of spectroscopy, though the most common types used for GF-NP based hybrid composite analysis include Fourier transform infrared spectroscopy, ultraviolet and visible spectroscopy and Raman spectroscopy.

3.2.1 Fourier Transform Infrared Spectroscopy

Fourier Transform Infrared Spectroscopy (FTIR) spectroscopy is used to demonstrate what kinds of bonds are present in a composite material by measuring at various frequencies different forms of interatomic bond vibrations [70, 146]. The FTIR spectra create a sample profile, a distinctive molecular fingerprint that can be used for screening and scanning nanofiller samples for different components based on G [12]. From an analytical point of view, by measuring the impact of molecular vibrations at the polymer and nanofiller interaction, the fraction of the interfacial polymer composite can be determined via FTIR spectroscopy [18, 147].

For instance, Pu et al. observed the characteristic FTIR spectra of GO and GO-TiO_2 nanohybrids (shown in Fig. 19) [148]. Both GO and GO-TiO_2 displayed spectra that have a large peak above 3000 cm^{-1}, resulting from the OH stretching vibrations of the H_2O and the C–OH groups [148]. GO displays the peaks for C=O at 1110 cm^{-1}, C–O–C at 1250 cm^{-1}, C–H at 1387 cm^{-1}, and C=O at 1720 cm^{-1} [148]. As for the hybrid GO-TiO_2 nanohybrid, the spectra for C=O disappeared completely, confirming the decomposition of partial oxygen comprising functional groups under microwave irradiation [148]. In addition, it was observed that the absorption edge of GO-TiO_2, relative to pure TiO_2, displayed an apparent shift [148]. This result indicated the narrowing of TiO_2's bandgap, which also supports the development of Ti–O–C bonds between GO and TiO_2 [148].

Figure 20 displays FTIR results for the main GO-SiO_2 hybrid filler (Fig. 20a) and the hybrid PLA composites (Fig. 20b) [12]. In addition to the predicted FTIR peaks for each filler in Fig. 20a, it was predicted that the peak at approximately 1420 cm^{-1} in the GO-SiO_2 nanohybrid originates from the -COOSi-group, which confirmed the desired connection between GO and silica [12]. Terzopoulou et al. used the FTIR results to compare a poly-lactic acid (PLA) composite structure when filled with hybrid fillers based on graphene and silica nanoparticles [12]. Figure 20b, particularly

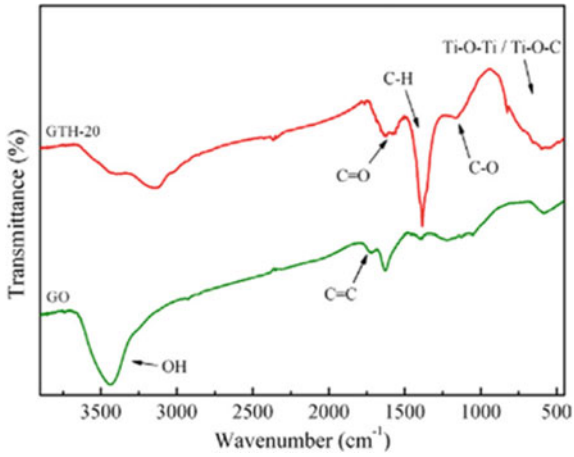

Fig. 19 FTIR spectra of raw GO and GO-TiO_2 nanohybrid [148]

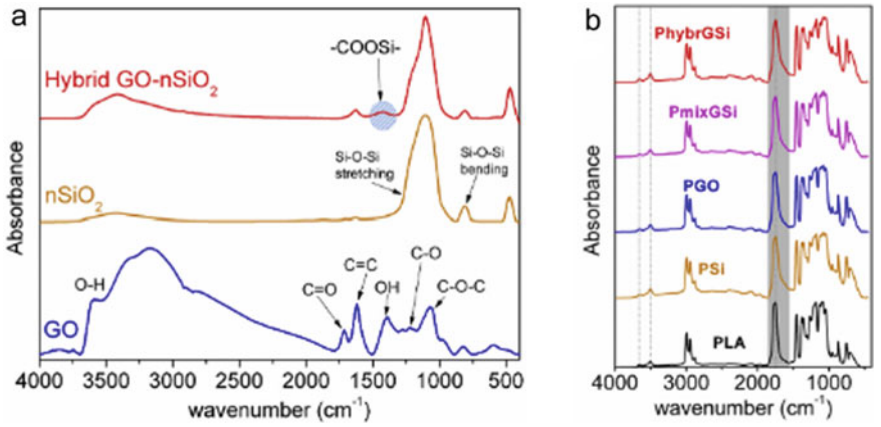

Fig. 20 Comparative FTIR spectra for **a** hybrid fillers GO-SiO_2 and **b** hybrid filler-based PLA composites. The major molecular vibrating groups leading to the spectra are colored grey [12]

the spectra around 1750 cm^{-1}, provided interesting information regarding the interactions between the polymer-fillers. The key sources of the peaks are the stretching and vibration of the PLA free carbonyl –C=O groups. The peak was clearly absent in the smooth GO and SiO_2 hybrid spectra (Fig. 20a), which affirms the polymer-filler interaction [12].

3.2.2 Ultraviolet-Visible Spectroscopy

In the same manner, as FTIR, Ultraviolet–visible spectroscopy (UV-Vis) technique applies to spectroscopy of absorption and reflectance within the section of

the ultraviolet and the complete, adjacent visible spectral region [149]. UV-vis-spectrophotometry was used as a function of light wavelength for determining light transmittance through graphene-based hybrid nanocomposite films [44, 150]. Furthermore, UV spectroscopy is an important method for the quantitative detection of various analytes in G based hybrid materials, such as transition metal ions (Cu, Au, Ag, Pb, Fe, Zn etc.) and conjugated organic compounds [22, 24, 151]. Such in the case of Wang et al. who analyzed the UV vis-à-vis spectra of rGO-TiO_2, rGO-Ag–TiO_2 and rGO-Pt–TiO_2 hybrids and found that all had a wide absorption range of 300–350 nm due to the TiO_2 absorption [151]. It was reported that the absorption in the rGO-Ag–TiO_2 nanohybrid spectrum at around 431 nm resulted from the excitation of a surface plasmon in noble metal nanoparticles and further confirmed the formation of Ag particles on the rGO-TiO_2 surface [151]. No apparent surface plasmon absorption was observed for the rGO-Pt–TiO_2 nanohybrid in the visible area [151].

UV-Vis spectrometry analysis was performed to investigate the electronic interaction of the G and nanometals (silver (Au) and gold (Ag)) [24]. Compared to the G spectra, additional peaks were observed for all the hybrids due to metal nanoparticles insertion [24]. Characteristic peaks at 545 and 410 nm were attributed respectively to Au and Ag surface plasmon resonance (SPR) [24], indicated the presence of Ag and Au nanoparticles on the surfaces of graphene. The G-AuAg's UV-Vis spectrum showed a strong absorption peak at 477 nm, which is noticeably different from G-Ag and G-Au hybrids peaks positions [24]. In order to study the conjugated structure of exfoliated graphene in G-CNF hybrid nanomaterials, UV-vis absorption spectra were analyzed for GO, rGO, and G-CNF [131]. As illustrated in Fig. 21, The UV-vis hybrid spectrum shows a high absorption peak of about 267 nm, close to that of rGO, whose conjugated graphic structure has been restored by chemical reduction, relative to that of GO [131].

UV-Visible spectrometry measured the anti-UV properties of polylactic acid (PLA) and nanocomposite films [44]. The pure PLA film absorbed strongly ultraviolet light (200–400 nm) and visible light (400–800 nm), by 92% transmittance [44]. Because of the combination of GO and ZnO nanoparticles, which increases the light

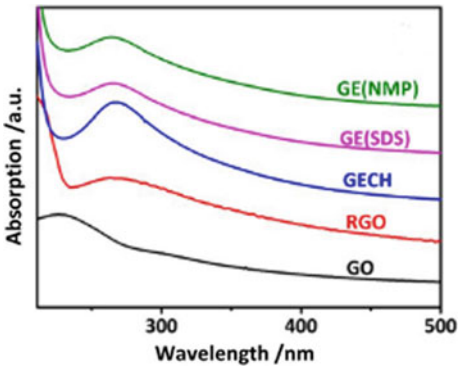

Fig. 21 UV-vis spectra of GO, rGO, G-CNF and exfoliated graphene obtained in N-Methyl-2-pyrrolidone (NMP) or in Sodium dodecyl sulfate (SDS) aqueous solution (presented in the graph as GO, RGO, GE (NMP) and GE (SDS), respectively) [131]

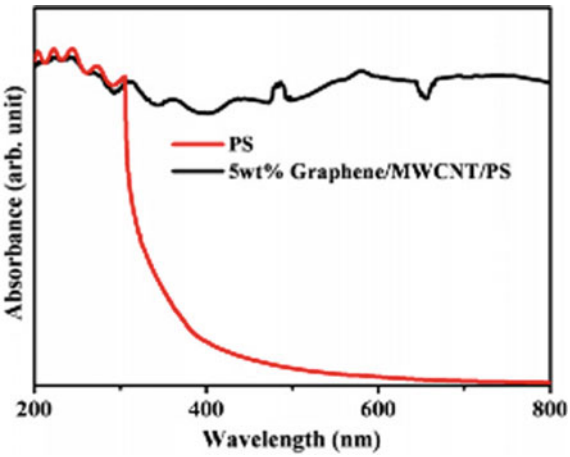

Fig. 22 UV-visible spectrum of neat and hybrid polystyrene (PS) nanocomposite [35]

absorption spectrum, the film displayed good anti-UV safety and good transmission of visible light when combined with GO-ZnO nanohybrid [44]. It was noticed that when the GO-ZnO content increases, the nanocomposite films obtain excellent absorption properties both in the UV region and in the visible region [44]. Similarly, in a study, Patole et al. presented UV-visible spectra of the polystyrene (PS) hybrid nanocomposite at wavelengths from 200 to 800 nm as shown in Fig. 22. PS spectra displayed peaks from lower to higher at approx. 200–400 nm led by associative interactions between the phenyl groups [35]. Similar peaks, less intense, appeared in the hybrid nanocomposite caused by addition of G-CNT hybrid, where the PS chains get tangled and trigger a screen effect limiting the absorption of the light beam [35].

3.2.3 Raman Spectroscopy

Raman spectroscopy is a valuable tool for performing carbon nanomaterials characterization, especially for identifying the order of graphene particles layers [75, 152]. Raman Spectroscopy was done to analyze the efficiency of the graphene nanosheets before and after a hybrid nanocomposite preparation [59]. Much information like grain boundaries, edge, disorder, doping, thickness, thermal conductivity and strain of graphene, can be obtained from the Raman spectrum and its characteristic s under various physical conditions [62, 68].

Considering the example in Fig. 23, Raman characterization that showed D band intensity ratios to G band (ID/IG) of GO, rGO, and G-CNT hybrid, which was around 0.97, 0.82, and 1.10, respectively [62]. These results confirmed that the amorphous carbon layer is formed during the CNT growth process [62]. In a different study, Das et al. analyzed the G-CNT hybrid's Raman spectrum, where all the typical carbon nanostructure bands (G, D, and 2D/2 G) were shown [153]. The full-width half maxima (FWHM) of 2D band were 30 for mono and bilayer graphene and 69.14 for

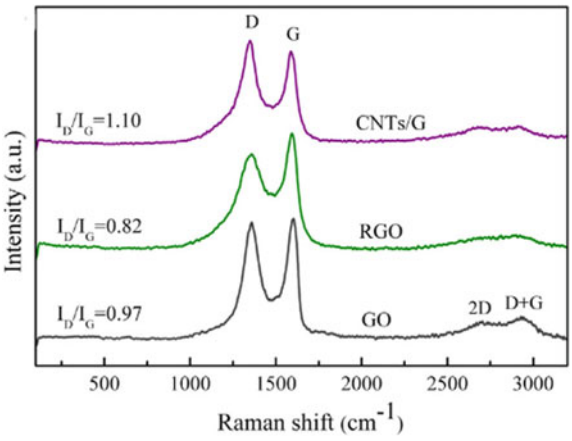

Fig. 23 Raman spectra of GO, RGO and G-CNT hybrid [62]

G-CNT [153]. It has been noted that the 2D peak enlargement can be attributed to the layer increase in the G architecture [153]. Likewise, the blue shift in the G-CNT hybrid band positions also suggested a relatively stronger bond between the G and CNT [153].

Xu et al. reported that G-metal contact, together with physisorption and chemisorption, cause the deviations of the G-band responses and the shifts of 2D-band frequency [154]. Furthermore, it was noted that the Cr, Ag and Al's interaction with G lead to a blueshift of the G peak, while Ni and Ti result in a redshift for the G peak [154]. The interactions of G and electrode metals like Ni, Ti, Al, Cr, and Ag introduced shifts in the peak G and the peak 2D [154]. Ni and Ti contributed to the peak G redshifts. Raman spectroscopy was reported to be an effective method for graphene studies, even if it interacts strongly with transition nanometal surfaces [154].

In another study, Raman analysis spectrum of GO displayed a D band at 1359 cm^{-1} as well as a G band at 1602 cm^{-1}, while the rGO-Co_3O_4 nanohybrid D and G bands were at 1330 cm^{-1} and 1596 cm^{-1}, respectively [9]. It was further noted that the redshift of the G band from 1602 to 1596 cm^{-1} for the rGO-Co_3O_4 nanohybrid was attributable to the recovery of the carbon atom's hexagonal network [9]. The nanohybrid rGO-Co_3O_4 exhibited a comparatively higher D-to-G-band intensity ratio (1.16) compared to the GO (0.96) [9]. Similarly, with regards to pure graphene D-to-G intensity ratio (0.497), the graphene-titanium dioxide hybrid D-to-G intensity ratio increased by 1.5 times (0.7) [155]. These results confirmed that after the chemical reduction of GO, there was the creation of a new graphitic domain [9, 155].

Research has been done using Raman spectroscopy to study the poly(pyronin Y) and the impact of rGO-silver (Ag) nanohybrid on the polymer [20]. It was observed that the rGO-Ag nanohybrid Raman spectrum resembles that of rGO sheet [20]. Furthermore, it was noticed that the ID/IG ratio for the rGO-Ag nanohybrid was 0.91, which was lower than that the rGO sheet, which may be an indication of Ag nanoparticles doping by filling the gaps left after extracting oxygen and iodine

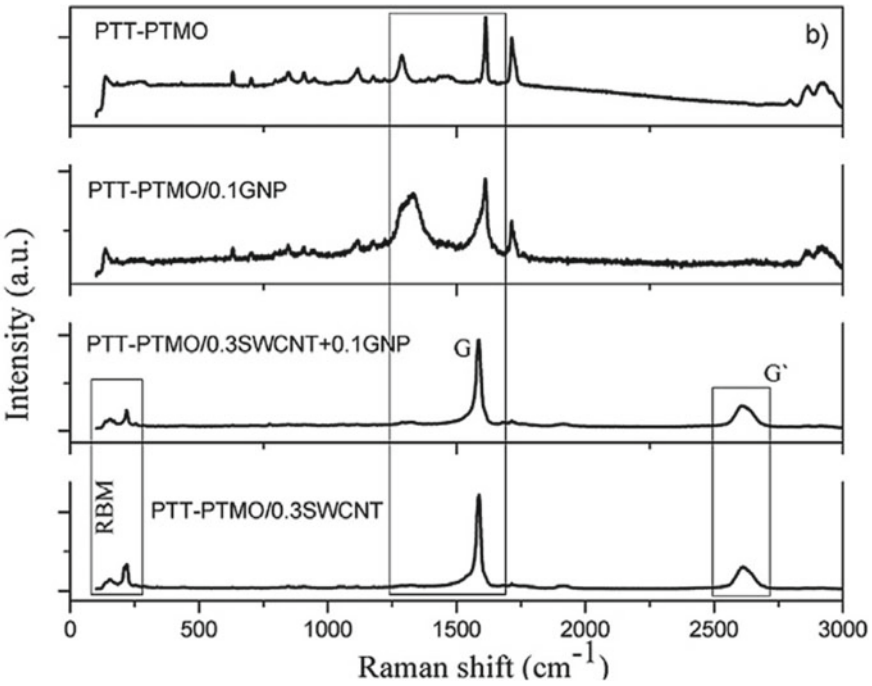

Fig. 24 Raman spectra of pure and hybrid PTT-PTMO [68]

molecules, decreasing the defect density [20]. Moreover, it was noted that for the poly(pyronin Y)/rGO-Ag hybrid nanocomposite Raman spectrum was considerably different than that of the fillers, due to the presence of poly (pyronin Y) as a matrix [20].

Raman spectroscopy was also performed for hybrid composites based on poly (trimethylene terephthalate-block-poly (Tetramethylene oxide) (PTT-PTMO) and G-CNT nanofillers as shown in Fig. 24 [68]. It was noted that the Raman spectrum corresponding to the hybrid nanocomposite with G-CNT hybrid nanofiller was almost similar to the nanocomposite with the CNT filler alone [68]. Therefore, CNT were proposed to be an indicator in deciding the properties of the hybrid nanocomposites [68]. In a different study, the structural study of the rGO, CNT, G-CNT, Polymethyl-methacrylate (PMMA), and PMMA/G-CNT hybrid composite was performed using Raman spectroscopy [16]. It was noted that PMMA Raman spectra display all of the typical PMMA peaks, except D and G bands [16]. After the G-CNT nanohybrid filler was integrated into the PMMA polymer matrix, D and G bands began to appear [16]. Furthermore, it was found that as the content of the G-CNT nanofiller increased, the intensity of the bands increased and showed a slight shift in peak position of the D and G bands, independent of the PMMA polymer peaks. This was related to chemical interactions between the PMMA polymer particles and the G-CNT nanohybrid filler particles [16].

3.3 X-Ray-Related Characterization

3.3.1 X-Ray Diffraction

X-ray methods are instrumental in providing data on the chemical composition and crystalline and amorphous structures of materials [40]. The X-ray Diffraction (XRD) and X-ray photoelectron spectroscopy (XPS) analysis are the most commonly used methods for characterizing composite hybrid materials [19, 151, 156]. XRD operates on the concept of diffraction from various planes of the atom generating a pattern of diffraction (diffractogram), that contains data of the atomic structure of the crystal. XRD is also used to detect a polymorph phase and determine the abundance of a phase to classify the hybrids and compare the compositional efficiency of composites [12, 151, 155].

Using XRD analysis of rGO-CNC nanohybrid, it was possible to confirm that the CNC were decorated on the rGO surface [40]. It was confirmed by noticing that after reduction, the strong (002) GO diffraction peak at $2\theta = 11.8°$ disappeared in the rGO and rGO-CNC hybrid [40]. Four defined diffraction peaks at 14.9, 16.6, 22.7 and 34.5° were reported, related to the presence of the crystalline region in the CNC and rGO-CNC nanohybrid, which suggests that the rGO-CNC crystalline structure is undamaged after GO reduction [40].

In another example, XRD was used to analyze and characterize the crystal structure patterns of the GO, rGO, Ni–Al alloy nanoparticles and an rGO-Ni–Al hybrid nanofiller (Fig. 25) [48]. It was observed that the GO's XRD pattern (Fig. 25) displayed a sharp peak at 10.48, suggesting the interplanar spacing of the (002) is around 0.85 nm, which is explained by the turbostratic structure of the stacked graphene plates [48]. The diffraction peaks (Fig. 25) of 11.48°, 23.18°, 35.28°, 39.38° and 46.58° correspond to the respective planes (003), (006), (012), (015) and (018), which is typical for a Ni–Al alloy hydrotalcite [48]. Furthermore, the XRD pattern

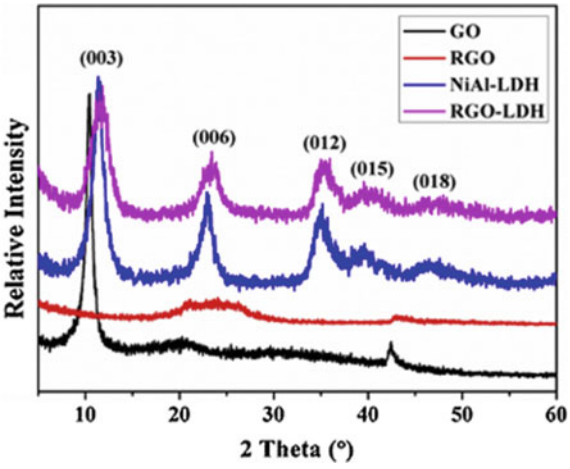

Fig. 25 XRD patterns of the obtained GO, rGO, Ni–Al layered double hydroxide and rGO-Ni–Al (rGO-LDH) [48]

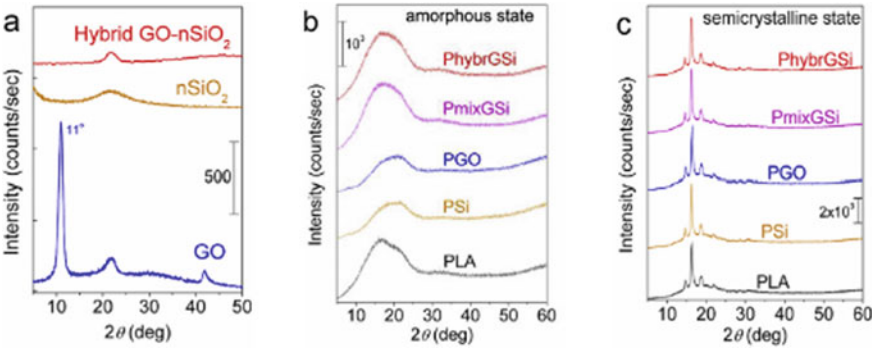

Fig. 26 XRD spectra for **a** the nanofiller particles (GO and SiO_2), and **b**, **c** pure polylactic acid (PLA) and PLA hybrid nanocomposite **b** amorphous and **c** semicrystalline nanocomposites [12]

of rGO-Ni–Al hybrid nanofiller is almost similar to that of pure Ni–Al alloy, and no characteristic peaks of the rGO are observed. These findings suggested that the Ni–Al alloy nanoparticles were well anchored on the rGO nanosheets, effectively preventing the graphene from being restacked [48].

In order to investigate the impact of integrating rGO and CNC on the crystallinity of the polylactic acid (PLA) matrix, the structure of CNC, the rGO filler and the neat PLA and rGO-CNC reinforced PLA nanocomposite were characterized by broad angle XRD analysis [78]. A broad diffraction band at $2\theta = 16.5°$ was depicted from the XRD spectra of the neat PLA polymer, suggesting a PLA's XRD-amorphous structure [78]. The XRD curves of the nanocomposite reinforced with rGO-CNC showed no peak of CNC and rGO at low filler contents, other than the wide prominent peak at $2\theta = 16.5°$, confirming a typical amorphous material [78].

In a different study, a polymer hybrid nanocomposite in its amorphous (melt-quenched) and semicrystalline (annealed) structures were investigated. Figure 26a displays the XRD spectrometers for the fillers separately and (Fig. 26b, c) for the nanocomposite [12]. Compared to the stuck-formed GO, it was confirmed that the complete exfoliation of the hybrid GO-SiO_2 was achieved [12]. This was confirmed by the absence of XRD peaks in the nanohybrid GO-SiO_2 at $2\theta \sim 10°$ in Fig. 26a. [12]. For the polymer hybrid nanocomposites, the XRD findings from Fig. 26b, c showed no observable alternations between the polymer matrix and the polymer hybrid nanocomposites in the reported XRD spectra [12]. Therefore, no significant alteration is observed in the crystalline structure of the neat polymer, nor in the polymer hybrid nanocomposites [12].

3.3.2 X-Ray Photoelectron Spectroscopy

X-ray photoelectron spectroscopy (XPS) is another method for the study of composite material's surface chemistry [157, 158]. The basic XPS principle is to irradiate

the surface of the studied material with X-rays to eject electrons from its surface [158]. The energy of these electrons, which is used to determine the surface chemical composition, is then measured [158]. XPS was used to analyze the elementary composition and the chemical state of a wide variety of solid samples from hybrids to composite materials [19, 49]. Besides, XPS was used in this study to determine the oxidation states of metal atoms, and the nitrogen bonding configuration of a G-$MnCo_2O_4$ nanohybrid [49]. It has been demonstrated that the observed characteristic peaks suggested that the hybrids contain carbon (C 1 s peak), oxygen (O 1 s peak), nitrogen (N 1 s peak), cobalt (Co 2p peak) and manganese (Mn 2p peak) elements and that the Co-to-Mn ratio is approximately 2 which was a close match to the modeled ratio [49]. Similarly, the chemical composition of rGO and rGO-Au nanohybrid was analyzed using XPS spectra of C1s and O1s [19]. XPS spectra of C1s and O1s, which confirmed the effective chemical reduction of GO and Au nanoparticles were present in the rGO-Au nanohybrid [19].

The XPS measurements confirmed the efficiency of the surface functionalization and the reduction of the hybrid nanofiller rGO-CNF [76]. Figure 27 shows that the intensity of the oxygen-containing group peaks for C1s binding region of rGO-CNF clearly decreased compared with that of the GO-CNF nanohybrid, indicating an efficient GO reduction [76].

Similarly, the surface chemical composition of the soy protein (SPI) hybrid nanocomposite films reinforced with GO-CNF and rGO-CNF were surveyed by XPS measurements [76]. The effective application of tannic acid coating on the SPI/GO-CNF structure was demonstrated in the SPI/rGO-CNF nanocomposite film spectrum by an increase in C1s and O1s peaks [76]. In addition, it was noted that the peak corresponding to the C=OH groups with rGO-CNF integration was significantly increased in the SPI/rGO-CNF nanocomposite film, which indicated the reaction potential of rGO-CNF with SPI matrix [76].

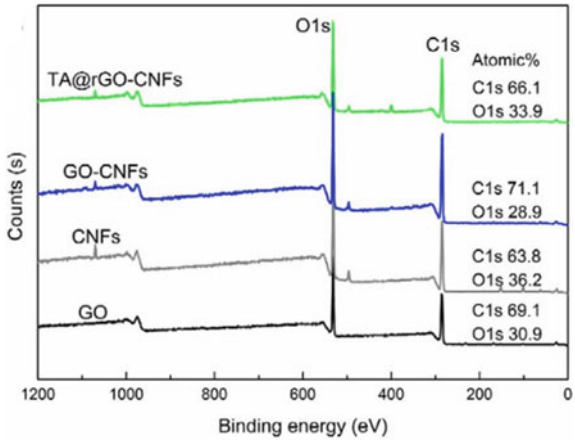

Fig. 27 Full XPS spectra **a** GO, CNFs, GO-CNFs and rGO-CNFs [76]

3.4 Thermal Analysis

3.4.1 Thermal Stability Analysis

Thermal analysis techniques are essential for a wide range of materials such as polymers, composites, pharmaceutical products, food packaging, fuels, energy, chemicals, and many more [70, 72]. These techniques, such as thermogravimetric analysis (TGA) and differential scanning calorimetry (DSC), usually measure heat transfer, weight loss, difference in size, or mechanical properties, as a function of change in temperature [156]. The thermogravimetric analysis (TGA) or derivative thermogravimetry (DTG) is an important laboratory tool used for the characterization of composite material. It measures the mass of material as temperature changes over time [159]. The TGA/DTG technique was used through the desired temperature range to provide insight into mass changes of G-NP hybrid and its nanocomposites [12, 31, 48, 159, 160]. In the case of the GO-CNT-CNF hybrid's, thermal stability was evaluated and two weight-loss mechanisms were demonstrated using TGA analysis [160]. It was found that a weight loss occurred in the temperature range 144−226 °C, due to the removal of oxygen-containing groups from the GO nanosheets [160]. Moreover, another weight loss was observed over the temperature range 233 − 413 °C, which agreed with the decomposition of the CNF in the GO-CNT-CNF hybrid [160]. In comparison, it was noted that in the TGA study of the rGO-CNT-CNF hybrid, there was only one weight loss phase, and it was correlated with the CNF decomposition. Such findings led to the interpretation that a successful reduction of the GO nanosheets to rGO [160].

Similarly, Tajik et al. examined the G-silica nanohybrid using TGA and DTG. They showed that there existed three thermally stable regions [159]. Due to its high percentage of silica phase, an effective thermal stability can be observed up to 549.06 °C at the first region [159]. Then, the second region was relevant to the abrupt reduction of sample weight from 549.06 to 629.78 °C likening it to the complete loss of G [159]. Therefore, the amount of G in the G-silica nanohybrid was roughly evaluated by the TGA and DTG analysis and was determined to be 16 wt% [159]. Hence, the TGA and DTG measurements have approved the formation of G nanosheet in the nanohybrid [159].

The TGA analysis was also used to characterize the thermal properties of the neat PVA film and the G-CNT hybrid nanofiller-reinforced PVA films at different hybrid filler ratio [31]. Both the neat PVA and the PVA hybrid composite films have been found to decompose through a two-step process [31]. First, a weight loss phase resulting from a thermal decomposition of PVA was estimated to take place at around 220–350 °C and a second step related to the thermal decomposition of the residue was considered to be at around 400–500 °C [31]. The TGA curve of the PVA hybrid nanocomposite film was shifted to a slightly higher temperature in comparison with that of the pure PVA film [31]. The PVA hybrid nanocomposite film peak temperatures at 314.4 and 440.3 °C, were approximately at 19.8 and 7.4 °C slightly higher than those of the neat PVA, which suggested to be due to enhanced compatibility

Table 1 TGA analysis data of PMMA neat polymer and PMMA reinforced with rGO, and Ni–Al alloy nanoparticles and rGo-NiAl hybrid nanofiller [48]

Sample	$T_{-5\%}$ (°C)	T_{max} (°C)	Residue at 750 °C (wt%)
PMMA	332	382	0.6
PMMA/rGO	320	384	1.4
PMMA/NiAl	326	386	2.2
PMMA/rGO-NiAl	330	380	3.7

between the PVA and the G-CNT hybrid nanofillers [31]. Similar findings were reported for the G-CNT as a hybrid reinforcement of poly(ether-ether-ketone) and poly(styrene-b-butadiene-b-styrene) [35, 112, 161].

TGA has further been used to analyze the effect of a rGO-Ni–Al hybrid on the thermal stability of the polymethyl methacrylate (PMMA) matrix as shown in the Table 1 [48]. Neat PMMA's thermal degradation demonstrated a single phase, and no residues were left [48]. It was remarked when rGO was added in the polymer matrix, the $T_{-5\%}$ (defined as the temperature where 5% of weight loss occurs) decreased by 12 °C because of the high thermal conductivity of rGO [48]. It was found that the maximum rate of decomposition decreases significantly, with the little residue possibly remaining because of the rGO that prevents the final thermal degradation of the polymer PMMA [48]. In the case of PMMA polymer reinforced with Ni–Al alloy, more char residue (2.2 wt%) remained, due to the catalytic carbonization effect of layered double hydroxide [48]. An improved thermal resilience of the PMMA polymer was achieved as demonstrated by a higher residue of 3.7 wt%, attributable to the combination of the rGO's physical barrier effect and the Ni–Al alloy's catalytic carbonization [48]. The TGA summary data of the PMMA neat polymer and the PMMA hybrid nanocomposite are given in Table 1.

3.4.2 Differential Scanning Analysis

Differential Scanning Calorimetry (DSC) is another thermal analysis method in which the heat flow in or out of a material is determined as a variable of temperature or time. In contrast, the material is exposed to a temperature-regulated system [35, 112]. DSC analysis was performed to evaluate the degree of crystallinity (X_c), the fusion heat (ΔHf) and the melting temperature (T_m) of graphene based nanohybrid composites [12, 15, 35, 40]. The degree of crystallinity (χ_c) is determined as follows: $\chi_c = \Delta H_m/\Delta H_0$ where ΔH_m is the evaluated melting enthalpy from DSC curves, and ΔH0 is the 100% crystalline melting enthalpy. In a study by Patole et al., DSC analysis were done to examined the impact of G-CNT hybrid filler in the thermal transformation of a segmental motion of the polystyrene (PS) polymeric chain [35]. It was observed that the existence of such a carbonaceous kind of filler enhanced thermal effect since the temperature needed to modify the behavior of the PS chains in hybrid nanocomposite from the glassy to the rubbery state was raised by 70 °C in comparison with the pure PS [35]. Furthermore, a high shoulder peak between 150

Table 2 Glass transition temperature (T_g) and melting conditions of PVA and its hybrid nanocomposite with a 0.5, 0.75 and 1.0 wt% reinforced G-CNT filler material [31]

	T_g (°C)	ΔH_m (J/g)	X_c (%)	T_m (°C)
PVA	77.3	67.24	48.5	221.24
PVA/0.5 wt% G-CNT	79.2	67.76	48.9	223.10
PVA/0.75 wt% G-CNT	80.3	67.68	48.8	223.92
PVA/1 wt% G-CNT	81.5	67.71	48.9	221.68

and 170 °C was also observed [35]. It was proposed that the thermal transformation started to become flexible from 150 °C due to the PS polymer chain at the edge of G, which was not fully covered by the carbonaceous fillers [35]. The shielding effect was caused by the presence of CNT, which is sandwiched between two graphene flakes and surrounded by the polymer chain PS [35].

Similarly, DSC analysis was used to evaluate the temperature of the glass transition (Tg) of pure PVA and its nanocomposite film, as summarized in Table 2 [31]. It was noted that PVA with 1 wt% G-CNT composite film exhibited 81.5 °C higher T_g than the pure PVA film (77.3 °C) [31]. The rise in T_g showed that PVA's successful attachment to graphene nanosheets limited the PVA chains' segmental motion [31]. It was further noted that there is a strong interfacial interaction between the G-CNT matrix and the PVA matrix, which benefits the successful transfer of load [31]. Correspondingly, For the GO-CNC hybrid nanofiller containing the high amount of GO (GO:CNC-2:1), the impact of nanofillers on the PVA's glass transition (T_g) and melting (T_m) temperatures from DSC is more significant because the (PVA-GO:CNC-2:1) exhibited a higher T_g and T_m compared to (PVA-GO:CNC-1:1) and (PVA-GO:CNC-1:2) [15].

3.5 Mechanical Characterization

3.5.1 Tensile Analysis

Polymer composites' mechanical properties rely on their structure at the nano- and micro-scales [31, 33, 109]. Generally, a good dispersion and a strong interfacial interaction between particles and the selected polymeric matrix induce superior mechanical properties of the polymer composite materials [30, 33, 106]. This was well attested by comparing the tensile stress–strain curves, highlighting that the compressive strength, Young's modulus and breaking elongation of well-dispersed G-NP hybrid composites are significantly higher than those observed for composites based on G or NP alone [11, 112, 161].

For instance, Fig. 28 demonstrates the tensile strength and the Young's modulus of polyvinyl chloride (PVC) film. It was noted that the Young's modulus with rGO-ZnO fillers varying from 5 to 20 wt% and PVC films with G-Zno hybrid fillers [11].

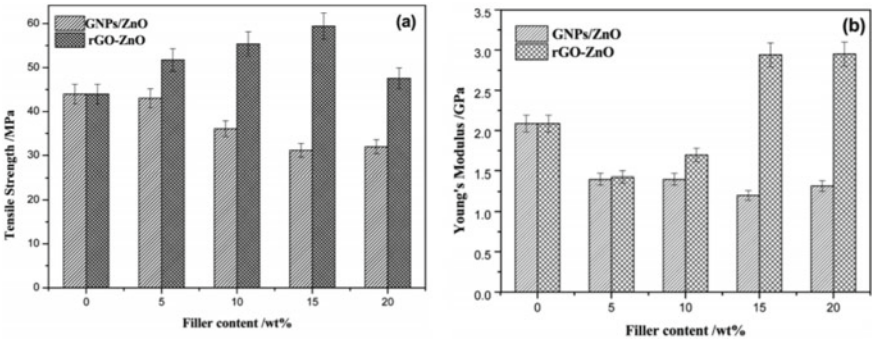

Fig. 28 **a** Tensile strength and **b** Young modulus of polyvinyl chloride (PVC) film incorporated with the specific ratio of G-ZnO and rGO-ZnO fillers [11]

Indeed, because of the poor interaction and aggregation of fillers, the tensile strength of PVC with G-ZnO fillers decreased with the increase of the filler material [11]. In comparison, it was found that PVC's tensile strength was obviously enhanced by adding rGO-ZnO hybrids, even at a high fillers content (20 wt%) [11]. It was also observed that the addition of G-ZnO hybrid particles had a negligible impact on the PVC's young modulus [11]. These results suggested that strong interfacial interaction occurred between rGO-ZnO hybrid particles and PVC chains but the interfacial interaction between G-ZnO hybrid particles and PVC chains were weak [11].

Several studies show that mechanical properties increased after reaching a critical GO-CNT content added into hybrid nanocomposites [129, 133]. Better mechanical properties could be achieved by using a homogenous dispersion and alignment, preventing the particles agglomeration and a better load transfer to filler material. For example, a uniaxial tensile measurement was used to investigate the mechanical properties of neat polyimide and its nanocomposites [129]. The tensile strength, Young modulus, toughness of fracture and strain at break of pure PI were found to be 74.3 MPa, 2.47 GPa, 12.71 MPa and 21.4%, respectively [129]. The strength and Young's modulus of the polyimide matrix were increased with the addition of GO, while the resilience of the strain at break and fracture significantly decreased [129]. However, by adding a small amount of CNT, the reinforcing efficiency of GO on polyimide was enhanced by 86%, 56%, 220% and 78% on the tensile strength, modulus, toughness and strain at break respectively, compared with those of the neat polyimide [129].

3.5.2 Dynamic Mechanical Analysis

Dynamic mechanical analysis (DMA) is the most useful tool for studying the viscoelastic condition of polymers and their composites [21, 30]. DMA analysis is defined as a function of temperature by the bending elastic modulus and damping

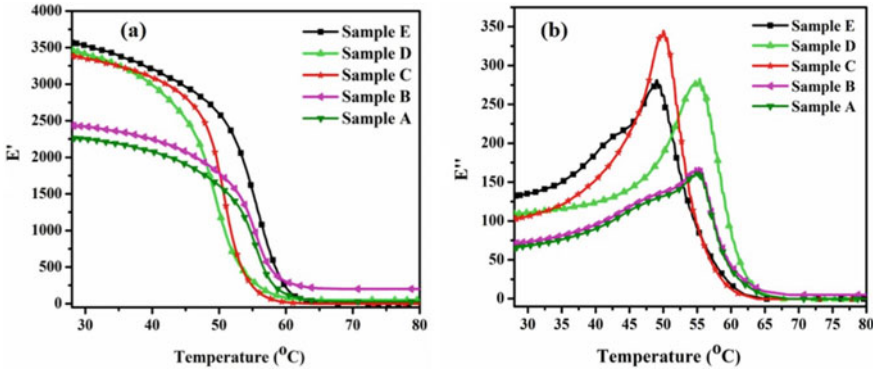

Fig. 29 E′ and E″ values obtained for the fabricated hybrid films obtained by DMA (Sample A: pure PLA and Sample B-E: PLA nanocomposite with G-CNC hybrid filler with ratio of 1:2, 1:4, 1:6 and 1:10 respectively) [38]

properties of the G-NP based hybrid composites. DMA analysis was used to study mechanical behaviors of polymers with different hybrid nanofillers such as G-CNT [161], G-SiC [162], G-TiO_2 [46], GO-CNT [112], rGO-CNC [38], etc. As a function of temperature in tensile mode, the dynamic mechanical behavior of the produced polylactic acid (PLA) hybrid nanocomposite films was calculated by DMA in terms of storage modulus (E') and loss modulus (E'') as shown in Fig. 29 [38]. By adding modified rGO-CNC hybrid in the PLA, it was observed that the E' values were enhanced by approximately 1.6 times for rGO-CNC based PLA compared to the neat PLA at 28 °C [38]. It was noted that the increase in E' values with increasing CNC concentration in the rGO-CNC hybrid could be related to the cross-related structure formation, enhancement of crystallinity (more organized regions formed) and better dispersion of rGO-CNC in the PLA matrix, resulting in improved adhesion between hybrid and polymer [38].

Similarly, the E' and loss factor (tanδ) of the studied G and CNC based natural rubber composites were investigated using DMA as a function of temperature (−30 to 80 °C) [39]. It was observed that the natural rubber composite filled with G, displayed the highest E' when the temperature was lower than the temperature of the glass transition [39]. It was also noted that natural rubber composites filled with CNC displayed a similar storage modules above the glass transition temperature (T_g) in comparison with the pure natural rubber [39]. It was concluded that the addition of G-CNC hybrid had no influence on the composites' glass transition temperature [39].

In other research works, the DMA findings showed a major enhancement of the E' and T_g in the GO-ZnO based poly-lactic acid (PLA) hybrid nanocomposite films [44]. The tanδ specified as the ratio of the loss module to the storage module displayed a peak around 60–80 °C corresponding to the glass transition of the PLA polymer chains [44]. The T_g values for pure PLA increased from 65.45 to 70.90 °C for the PLA nanocomposite reinforced with 0.5 wt% GO-ZnO filler [44]. Furthermore,

it was reported that this effect was caused by the large specific surface area of the GO sheets and the reinforcement effect of loaded ZnO nanoparticles on the GO surfaces, strong interfacial action was effectively created and the mobility of PLA chains was reduced [44].

4 Conclusion

The characterization of hybrid nanocomposites is fundamental to obtain important information on these materials, such as: (1) the hybrid filler distribution in the polymer matrix, (2) the effect of the filler surface modification on the filler dispersion and composite properties, (3) interactions of the hybrid filler with the polymer chains, (4) changes in the process parameters on the resulting morphology and properties, (5) broad range of properties to establish potential applications of nanocomposites. This chapter has provided the advances on recent characterization techniques for the nanocomposites specifically prepared by the incorporation of G-NP as hybrid fillers.

Major categories of hybrid fillers and nanocomposites based on G and NP were also briefly summarized in their preparation and proposed chemical structures. The exceptional morphological, chemical, thermal, and mechanical properties demonstrated for hybrids of G-NP make of them an excellent candidate for strengthening nanocomposites. It is also worth noting that different G-NP hybrid fillers influence high specific properties such as mechanical and thermal properties of the polymeric matrix, but how effective the influence is based solely on their degree of dispersion within the matrix because agglomeration of the hybrid nanofillers significantly reduces or causes more detrimental impact on the hybrid nanocomposite.

The most significant characterization techniques in this field of research were reviewed and the relevant literature existing for G-NP based polymer nanocomposites was highlighted. Hence, attention was given to the numerous methods of analysis in the available literature such as the microscopy techniques SEM, TEM, HRTEM and AFM, spectroscope technologies (FTIR, UV-vis and Raman), X-ray related analysis (XRD and XPS), Thermal analysis (TGA/DTG and DSC) and mechanical characterization methods.

Recent studies of fillers and nanocomposite based on G-NP have been represented using various microscopic techniques, such as SEM, TEM, and AFM. The capabilities of each microscopy technique allow for analysis of various aspects of hybrid fillers and nanocomposites. It was also highlighted that the information obtained by the spectroscopic techniques (FTIR, UV-vis and Raman) involves a number of aspects, such as the chemical composition of the samples, the binding of the surfactants to the surface of the nanoparticles, the intercalation of the modifiers in the basal spacing of the hybrid fillers and the presence of an intermolecular interaction between the hybrid nanofillers and the polymer matrix. In the case where the optical behavior of nanocomposites is defined, UV-vis analysis is performed, which shows the peak wavelength.

For the X-ray based characterization, XRD was used to measure the effectiveness of the filler on crystallization and lamella thickness. In contrast, XPS was used to investigate a wide variety of surface modifications on graph fillers and polymeric materials. Thermal analysis is essential to the design of materials for heat management services: because thermal properties of a composite material boost and guarantee a system's service life as well as reduce hazard. At the same time, mechanical characterization is important to understand hybrid nanocomposite characteristics in advanced applications such as packaging, automotive, sensor technology and other thermomechanical facilities. All of these techniques will be suitable and essential to understanding the better formulation of G-NP based hybrid composites for a wide range of different technological applications. The developments in the above methods will provide more knowledge in this field in the near future, as well as greater insight into G-NP based hybrid fillers and composites structures.

References

1. Khin MM, Nair AS, Babu VJ, Murugan R, Ramakrishna S (2012) A review on nanomaterials for environmental remediation. Energy Environ Sci 5(8):8075–8109
2. Kassab Z, Abdellaoui Y, Salim MH, El Achaby M (2020) Cellulosic materials from pea (Pisum Sativum) and broad beans (Vicia Faba) pods agro-industrial residues. Mater Lett 280:128539
3. Kassab Z, Abdellaoui Y, Salim MH, Bouhfid R, Qaiss AEK, El Achaby M (2020) Micro- and nano-celluloses derived from hemp stalks and their effect as polymer reinforcing materials. Carbohydr Polym 245:116506
4. Gunjakar JL, Kim IY, Lee JM, Jo YK, Hwang SJ (2014) Exploration of nanostructured functional materials based on hybridization of inorganic 2D nanosheets. J Phys Chem C 118(8):3847–3863
5. Devi MM, Sahu SR, Mukherjee P, Sen P, Biswas K (2015) Graphene: a self-reducing template for synthesis of graphene-nanoparticles hybrids. RSC Adv 5(76):62284–62289
6. Kumar S, Raj S, Jain S, Chatterjee K (2016) Multifunctional biodegradable polymer nanocomposite incorporating graphene-silver hybrid for biomedical applications. Mater Des 108:319–332
7. Mittal G, Dhand V, Rhee KY, Park SJ, Lee WR (2015) A review on carbon nanotubes and graphene as fillers in reinforced polymer nanocomposites. J Ind Eng Chem 21:11–25 (Korean Society of Industrial Engineering Chemistry)
8. Tabandeh-Khorshid M, Kumar A, Omrani E, Kim C, Rohatgi P (2020) Synthesis, characterization, and properties of graphene reinforced metal-matrix nanocomposites. Compos Part B: Eng 183:107664 (Elsevier Ltd.)
9. Wang GS et al (2014) Fabrication of reduced graphene oxide (RGO)/Co_3O_4 nanohybrid particles and a RGO/Co_3O_4/poly(vinylidene fluoride) composite with enhanced wave-absorption properties. ChemPlusChem 79(3):375–381
10. Cho BG, Lee S, Hwang SH, Han JH, Chae HG, Bin Park Y (2018) Influence of hybrid graphene oxide-carbon nanotube as a nano-filler on the interfacial interaction in nylon composites prepared by in situ interfacial polymerization. Carbon NY 140:324–337
11. Li P, Chen X, Zeng JB, Gan L, Wang M (2016) Enhancement of the interfacial interaction between poly(vinyl chloride) and zinc oxide modified reduced graphene oxide. RSC Adv 6(7):5784–5791
12. Terzopoulou Z et al (2019) Interfacial interactions, crystallization and molecular mobility in nanocomposites of Poly(lactic acid) filled with new hybrid inclusions based on graphene oxide and silica nanoparticles. Polymer (Guildf) 166:1–12

13. Zhang J et al (2014) Magnetic and mechanical properties of polyvinyl alcohol (PVA) nanocomposites with hybrid nanofillers—Graphene oxide tethered with magnetic Fe_3O_4 nanoparticles. Chem Eng J 237:462–468
14. Chatterjee S, Nafezarefi F, Tai NH, Schlagenhauf L, Nüesch FA, Chu BTT (2012) Size and synergy effects of nanofiller hybrids including graphene nanoplatelets and carbon nanotubes in mechanical properties of epoxy composites. Carbon NY 50(15):5380–5386
15. El Miri N et al (2016) Synergistic effect of cellulose nanocrystals/graphene oxide nanosheets as functional hybrid nanofiller for enhancing properties of PVA nanocomposites. Carbohydr Polym 137:239–248
16. Mishra SK, Tripathi SN, Choudhary V, Gupta BD (2015) Surface Plasmon resonance-based fiber optic methane gas sensor utilizing graphene-carbon nanotubes-poly(methyl methacrylate) hybrid nanocomposite. Plasmonics 10(5):1147–1157
17. Du X, Zhou M, Deng S, Du Z, Cheng X, Wang H. Poly(ethylene glycol)-grafted nanofibrillated cellulose/graphene hybrid aerogels supported phase change composites with superior energy storage capacity and solar-thermal conversion efficiency. Cellulose 27
18. Fakhri P, Mahmood H, Jaleh B, Pegoretti A (2016) Improved electroactive phase content and dielectric properties of flexible PVDF nanocomposite films filled with Au- and Cu-doped graphene oxide hybrid nanofiller. Synth Met 220:653–660
19. Wang Y et al (2011) Self assembly of acetylcholinesterase on a gold nanoparticles-graphene nanosheet hybrid for organophosphate pesticide detection using polyelectrolyte as a linker. J Mater Chem 21(14):5319–5325
20. Da¸cl K, Alanyallo¸lu M (2016) Preparation of free-standing and flexible graphene/Ag nanoparticles/poly(pyronin Y) hybrid paper electrode for amperometric determination of nitrite. ACS Appl Mater Interfaces 8(4):2713–2722
21. Huang X, Zhao G, Wang X (2015) Fabrication of reduced graphene oxide/metal (Cu, Ni, Co) nanoparticle hybrid composites via a facile thermal reduction method. RSC Adv. 5(62):49973–49978
22. Li J et al (2015) Bimetallic Ag–Pd nanoparticles-decorated graphene oxide: A fascinating three-dimensional nanohybrid as an efficient electrochemical sensing platform for vanillin determination. Electrochim Acta 176:827–835
23. Gao T, Chen L, Li Z, Yu L, Wu Z, Zhang Z (2016) Preparation of zinc hydroxystannate-decorated graphene oxide nanohybrids and their synergistic reinforcement on reducing fire hazards of flexible poly (vinyl chloride). Nanoscale Res Lett 11(1):1–10
24. Manolata Devi M, Sahu SR, Mukherjee P, Sen P, Biswas K (2016) Graphene–metal nanoparticle hybrids: electronic interaction between graphene and nanoparticles. Trans Ind Inst Met 69(4):839–844
25. Sun Y, Zheng H, Wang C, Yang M, Zhou A, Duan H (2016) Ultrasonic-electrodeposition of PtPd alloy nanoparticles on ionic liquid-functionalized graphene paper: towards a flexible and versatile nanohybrid electrode. Nanoscale 8(3):1523–1534
26. Liu T, Li C, Yuan Q (2018) Facile synthesis of PtCu alloy/graphene oxide hybrids as improved electrocatalysts for alkaline fuel cells. ACS Omega 3(8):8724–8732
27. Ren F et al (2018) Synergistic effect of graphene nanosheets and carbonyl iron-nickel alloy hybrid filler on electromagnetic interference shielding and thermal conductivity of cyanate ester composites. J Mater Chem C 6(6):1476–1486
28. Shang L, Zhao F, Zeng B (2014) 3D porous graphene-porous PdCu alloy nanoparticles-molecularly imprinted poly(para-aminobenzoic acid) composite for the electrocatalytic assay of melamine. ACS Appl Mater Interfaces 6(21):18721–18727
29. Jiang Q, Wang X, Zhu Y, Hui D, Qiu Y (2014) Mechanical, electrical and thermal properties of aligned carbon nanotube/polyimide composites. Compos Part B Eng. 56:408–412
30. Yang Z, Li Q, Tong Y, Wu T, Feng Y (2019) Homogeneous dispersion of multiwalled carbon nanotubes via in situ bubble stretching and synergistic cyclic volume stretching for conductive LDPE/MWCNTs nanocomposites. Polym Eng Sci 59(10):2072–2081
31. Ma HL et al (2014) Radiation preparation of graphene/carbon nanotubes hybrid fillers for mechanical reinforcement of poly(vinyl alcohol) films. Radiat Phys Chem 118:21–26

32. Zhang S, Yin S, Rong C, Huo P, Jiang Z, Wang G (2013) Synergistic effects of functionalized graphene and functionalized multi-walled carbon nanotubes on the electrical and mechanical properties of poly(ether sulfone) composites. Eur Polym J 49(10):3125–3134
33. Qian Z, Song J, Liu Z, Peng Z (2019) Improving mechanical properties and thermal conductivity of styrene-butadiene rubber via enhancing interfacial interaction between rubber and graphene oxide/carbon nanotubes hybrid. Macromol Res 27(11):1136–1143
34. Zhu Z (2017) An overview of carbon nanotubes and graphene for biosensing applications. Nano-Micro Lett. 9(3):1–24
35. Patole AS, Patole SP, Jung SY, Yoo JB, An JH, Kim TH (2012) Self assembled graphene/carbon nanotube/polystyrene hybrid nanocomposite by in situ microemulsion polymerization. Eur Polym J 48(2):252–259
36. David L, Feldman A, Mansfield E, Lehman J, Singh G (2014) Evaluating the thermal damage resistance of graphene/carbon nanotube hybrid composite coatings. Sci Rep 4:1–6
37. Kassab Z, Aziz F, Hannache H, Ben Youcef H, El Achaby M (2019) Improved mechanical properties of k-carrageenan-based nanocomposite films reinforced with cellulose nanocrystals. Int J Biol Macromol 123:1248–1256
38. Pal N, Banerjee S, Roy P, Pal K (2019) Reduced graphene oxide and PEG-grafted TEMPO-oxidized cellulose nanocrystal reinforced poly-lactic acid nanocomposite film for biomedical application. Mater Sci Eng C 104:109956
39. Lin L et al (2018) Study on the impact of graphene and cellulose nanocrystal on the friction and wear properties of SBR/NR composites under dry sliding conditions. Wear 414–415:43–49
40. Ye YS et al (2016) Biocompatible reduced graphene oxide sheets with superior water dispersibility stabilized by cellulose nanocrystals and their polyethylene oxide composites. Green Chem 18(6):1674–1683
41. Oraon R, De Adhikari A, Tiwari SK, Nayak GC (2015) Nanoclay based graphene polyaniline hybrid nanocomposites: promising electrode materials for supercapacitors. RSC Adv 5(84):68334–68344
42. Trifol J, Plackett D, Sillard C, Szabo P, Bras J, Daugaard AE (2016) Hybrid poly(lactic acid)/nanocellulose/nanoclay composites with synergistically enhanced barrier properties and improved thermomechanical resistance. Polym Int 65(8):988–995
43. Walimbe P, Chaudhari M (2019) State-of-the-art advancements in studies and applications of graphene: a comprehensive review. Mater Today Sustain 6:100026 (Elsevier Ltd.)
44. Huang Y et al (2015) Poly(lactic acid)/graphene oxide-ZnO nanocomposite films with good mechanical, dynamic mechanical, anti-UV and antibacterial properties. J Chem Technol Biotechnol 90(9):1677–1684
45. Wang C et al (2017) Silver nanoparticles/graphene oxide decorated carbon fiber synergistic reinforcement in epoxy-based composites. Polymer (Guildf) 131:263–271
46. Feng X, Xing W, Song L, Hu Y, Liew KM (2015) TiO_2 loaded on graphene nanosheet as reinforcer and its effect on the thermal behaviors of poly(vinyl chloride) composites. Chem Eng J 260:524–531
47. Wang S et al (2013) Ionic-liquid-assisted facile synthesis of silver nanoparticle-reduced graphene oxide hybrids by gamma irradiation. Carbon NY 55:245–252
48. Hong N et al (2014) Co-precipitation synthesis of reduced graphene oxide/NiAl-layered double hydroxide hybrid and its application in flame retarding poly(methyl methacrylate). Mater Res Bull 49(1):657–664
49. Wang D, Zhang Q, Zhou K, Yang W, Hu Y, Gong X (2014) The influence of manganese-cobalt oxide/graphene on reducing fire hazards of poly(butylene terephthalate). vol 278. Elsevier B.V.
50. Zhang S et al (2011) Graphene decorated with PtAu alloy nanoparticles: Facile synthesis and promising application for formic acid oxidation. Chem Mater 23(5):1079–1081
51. Chen Q, Liu P, Sheng C, Zhou L, Duan Y, Zhang J (2014) Tunable self-assembly structure of graphene oxide/cellulose nanocrystal hybrid films fabricated by vacuum filtration technique. RSC Adv 4(74):39301–39304
52. Mani V, Govindasamy M, Chen SM, Karthik R, Huang ST (2016) Determination of dopamine using a glassy carbon electrode modified with a graphene and carbon nanotube hybrid decorated with molybdenum disulfide flowers. Microchim Acta 183(7):2267–2275

53. Mwafy EA, Mostafa AM (2019) Multi walled carbon nanotube decorated cadmium oxide nanoparticles via pulsed laser ablation in liquid media. Opt Laser Technol 111(September 2018):249–254
54. Venkatesan S, Visvalingam B, Mannathusamy G, Viswanathan V, Rao AG (2018) Effect of chemical vapor deposition parameters on the diameter of multi-walled carbon nanotubes. Int Nano Lett 8(4):297–308
55. Che J, Jing M, Liu D, Wang K, Fu Q (2018) Largely enhanced thermal conductivity of HDPE/boron nitride/carbon nanotubes ternary composites via filler network-network synergy and orientation. Compos Part A Appl Sci Manuf 112:32–39
56. Che J, Wu K, Lin Y, Wang K, Fu Q (2017) Largely improved thermal conductivity of HDPE/expanded graphite/carbon nanotubes ternary composites via filler network-network synergy. Compos Part A Appl Sci Manuf 99:32–40
57. Belmonte M, Nistal A, Boutbien P, Román-Manso B, Osendi MI, Miranzo P (2016) Toughened and strengthened silicon carbide ceramics by adding graphene-based fillers. Scr Mater 113:127–130
58. Fatemi SM, Foroutan M (2016) Recent developments concerning the dispersion of carbon nanotubes in surfactant/polymer systems by MD simulation. J Nanostructure Chem 6(1):29–40
59. Xu J et al (2018a) A review of functionalized carbon nanotubes and graphene for heavy metal adsorption from water: preparation, application, and mechanism. Chemosphere 195:351–364
60. Wen L, Li F, Cheng HM (2016) Carbon nanotubes and graphene for flexible electrochemical energy storage: from materials to devices. Adv Mater 28(22):4306–4337
61. Deng L, Gu Y, Gao Y, Ma Z, Fan G (2017) Carbon nanotubes/holey graphene hybrid film as binder-free electrode for flexible supercapacitors. J Colloid Interface Sci 494:355–362
62. Kong L et al (2014) Electromagnetic wave absorption properties of graphene modified with carbon nanotube/poly(dimethyl siloxane) composites. Carbon NY 73:185–193
63. Wang E et al (2019) Effect of graphene oxide-carbon nanotube hybrid filler on the mechanical property and thermal response speed of shape memory epoxy composites. Compos Sci Technol 169:209–216
64. Verma M, Chauhan SS, Dhawan SK, Choudhary V (2017) Graphene nanoplatelets/carbon nanotubes/polyurethane composites as efficient shield against electromagnetic polluting radiations. Compos Part B Eng 120:118–127
65. Wang C, Yang S, Ma Q, Jia X, Ma PC (2017) Preparation of carbon nanotubes/graphene hybrid aerogel and its application for the adsorption of organic compounds. Carbon NY 118:765–771
66. Dasgupta A, Rajukumar LP, Rotella C, Lei Y, Terrones M (2017) Covalent three-dimensional networks of graphene and carbon nanotubes: synthesis and environmental applications. Nano Today 12:116–135
67. Jun Xiao Y et al (2016) Hybrid network structure and thermal conductive properties in poly(vinylidene fluoride) composites based on carbon nanotubes and graphene nanoplatelets. Compos Part A Appl Sci Manuf 90:614–625
68. Paszkiewicz S et al (2015) Synergetic effect of single-walled carbon nanotubes (SWCNT) and graphene nanoplatelets (GNP) in electrically conductive PTT-block-PTMO hybrid nanocomposites prepared by in situ polymerization. Compos Sci Technol 118:72–77
69. Zhang C, Huang S, Tjiu WW, Fan W, Liu T (2012) Facile preparation of water-dispersible graphene sheets stabilized by acid-treated multi-walled carbon nanotubes and their poly(vinyl alcohol) composites. J Mater Chem 22(6):2427–2434
70. Kassab Z, Syafri E, Tamraoui Y, Hannache H, Qaiss AEK, El Achaby M (2019) Characteristics of sulfated and carboxylated cellulose nanocrystals extracted from Juncus plant stems. Int J Biol Macromol
71. El Achaby M, Kassab Z, Barakat A, Aboulkas A (2018) Alfa fibers as viable sustainable source for cellulose nanocrystals extraction: application for improving the tensile properties of biopolymer nanocomposite films. Ind Crops Prod 112:499–510
72. El Achaby M, Kassab Z, Aboulkas A, Gaillard C, Barakat A (2018) Reuse of red algae waste for the production of cellulose nanocrystals and its application in polymer nanocomposites. Int J Biol Macromol 106:681–691

73. Kassab Z et al (2020) Identifying Juncus plant as viable source for the production of micro- and nano-cellulose fibers: application for PVA composite materials development. Ind Crops Prod 144(December 2019):112035
74. Kassab Z, Kassem I, Hannache H, Bouhfid R, Qaiss AEK, El Achaby M (2020) Tomato plant residue as new renewable source for cellulose production: extraction of cellulose nanocrystals with different surface functionalities. Cellulose 7:1–17
75. Terrones M et al (2010) Graphene and graphite nanoribbons: morphology, properties, synthesis, defects and applications. Nano Today 5(4):351–372 (Elsevier B.V.)
76. Wang Z, Kang H, Zhao S, Zhang W, Zhang S, Li J (2018) Polyphenol-induced cellulose nanofibrils anchored graphene oxide as nanohybrids for strong yet tough soy protein nanocomposites. Carbohydr Polym 180:354–364
77. Cao J, Zhang X, Wu X, Wang S, Lu C (2016) Cellulose nanocrystals mediated assembly of graphene in rubber composites for chemical sensing applications. Carbohydr Polym 140:88–95
78. Pal N, Dubey P, Gopinath P, Pal K (2017) Combined effect of cellulose nanocrystal and reduced graphene oxide into poly-lactic acid matrix nanocomposite as a scaffold and its anti-bacterial activity. Int J Biol Macromol 95:94–105
79. Xu S, Yu W, Yao X, Zhang Q, Fu Q (2016) Nanocellulose-assisted dispersion of graphene to fabricate poly(vinyl alcohol)/graphene nanocomposite for humidity sensing. Compos Sci Technol 131:67–76
80. Montes S et al (2015) Synergistic reinforcement of poly(vinyl alcohol) nanocomposites with cellulose nanocrystal-stabilized graphene. Compos Sci Technol 117:26–31
81. Zabihi O, Ahmadi M, Nikafshar S, Chandrakumar Preyeswary K, Naebe M (2018) A technical review on epoxy-clay nanocomposites: Structure, properties, and their applications in fiber reinforced composites. Compos Part B: Eng 135:1–24 (Elsevier Ltd.)
82. Panwar V, Chattree A, Pal K (2017) Effect of nanoclay on thermomechanical behaviour of graphene oxide/polymer composites. Procedia Eng 216:101–110
83. Adrar S, Habi A, Ajji A, Grohens Y (2018) Synergistic effects in epoxy functionalized graphene and modified organo-montmorillonite PLA/PBAT blends. Appl Clay Sci 157(February):65–75
84. Zhan Y, He S, Wan X, Zhao S, Bai Y (2018) Thermally and chemically stable poly(arylene ether nitrile)/halloysite nanotubes intercalated graphene oxide nanofibrous composite membranes for highly efficient oil/water emulsion separation in harsh environment. 567 (Elsevier B.V.)
85. Oraon R, De Adhikari A, Tiwari SK, Sahu TS, Nayak GC (2015) Fabrication of nanoclay based graphene/polypyrrole nanocomposite: An efficient ternary electrode material for high performance supercapacitor. Appl Clay Sci 118:231–238
86. Bouakaz BS, Pillin I, Habi A, Grohens Y (2015) Synergy between fillers in organomontmorillonite/graphene-PLA nanocomposites. Appl Clay Sci 116–117:69–77
87. Mia X et al (2019) Fabrication of halloysite nanotubes/reduced graphene oxide hybrids for epoxy composites with improved thermal and mechanical properties. Polym Test 76(April):473–480
88. Liu C, Yu L, Zhang Y, Zhang B, Liu J, Zhang H (2013) Preparation of poly(sodium acrylate-acrylamide) superabsorbent nanocomposites incorporating graphene oxide and halloysite nanotubes. RSC Adv 3(33):13756–13763
89. Li S, Yang Z, Xu J, Xie J (2018) Montmorillonite–graphene oxide hybrids and montmorillonite–graphene oxide/epoxy composite: synthesis, characterization, and properties. Polym Compos 39:E2084–E2095
90. Senthilnathan J, Sanjeeva Rao K, Lin WH, Der Liao J, Yoshimura M (2014) Low energy synthesis of nitrogen functionalized graphene/nanoclay hybrid via submerged liquid plasma approach. Carbon NY 78:446–454
91. Zhao C, Lv J, Xu X, Zhang G, Yang Y, Yang F (2017) Highly antifouling and antibacterial performance of poly (vinylidene fluoride) ultrafiltration membranes blending with copper oxide and graphene oxide nanofillers for effective wastewater treatment. J Colloid Interface Sci 505:341–351

92. Bindu Sharmila TK, Antony JV, Jayakrishnan MP, Sabura Beegum PM Thachil ET (2016) Mechanical, thermal and dielectric properties of hybrid composites of epoxy and reduced graphene oxide/iron oxide. Mater Des 90:66–75
93. Huang YL et al (2012) Self-assembly of silver-graphene hybrid on electrospun polyurethane nanofibers as flexible transparent conductive thin films. Carbon NY 50(10):3473–3481
94. Zhang L, Han G, Liu Y, Tang J, Tang W (2014) Immobilizing haemoglobin on gold/graphene-chitosan nanocomposite as efficient hydrogen peroxide biosensor. Sens Actuat B Chem 197:164–171
95. He F, Lam K, Ma D, Fan J, Chan LH, Zhang L (2013) Fabrication of graphene nanosheet (GNS)-Fe_3O_4 hybrids and GNS- Fe_3O_4/syndiotactic polystyrene composites with high dielectric permittivity. Carbon NY 58:175–184
96. Xia BY, Yan Y, Li N, Bin H, Wu B, Lou XWD, Wang X (2016) A metal-organic framework-derived bifunctional oxygen electrocatalyst. Nat Energy 1(1):1–8
97. Fernandes R, Patel N, Miotello A, Jaiswal R, Kothari DC (2011) Stability, durability, and reusability studies on transition metal-doped Co–B alloy catalysts for hydrogen production. Int J Hydrogen Energy 36(21):13379–13391
98. Vinayan BP, Ramaprabhu S (2013) Platinum-TM (TM=Fe,Co) alloy nanoparticles dispersed nitrogen doped (reduced graphene oxide-multiwalled carbon nanotube) hybrid structure cathode electrocatalysts for high performance PEMFC applications. Nanoscale 5(11):5109–5118
99. Jia X, Guan Q, Chen Y, Wang Y, Zhao Q, Li J (2019) Poly (triazine imide) (PTI) and graphene hybrids supported Pt[sbnd]Sn catalysts for enhanced electrocatalytic oxidation of ethanol. Appl Surf Sci 492(June):879–885
100. Nan X, Ma J, Liu J, Zhao J, Zhu W (2016) Effect of surfactant functionalization of multi-walled carbon nanotubes on mechanical, electrical and thermal properties of epoxy nanocomposites. Fibers Polym 17(11):1866–1874
101. Cai D, Song M (2010) Recent advance in functionalized graphene/polymer nanocomposites. J Mater Chem 20(37):7906–7915
102. Cui Y, Kundalwal SI, Kumar S (2016) Gas barrier performance of graphene/polymer nanocomposites. Carbon NY 98:313–333
103. Kim H, Abdala AA, MacOsko CW (2010) Graphene/polymer nanocomposites. Macromolecules 43(16):6515–6530
104. Kurapati R, Kostarelos K, Prato M, Bianco A (2016) Biomedical uses for 2D materials beyond graphene: current advances and challenges ahead. Adv Mater 28(29):6052–6074
105. Byrne MT, Guin'Ko YK (2010) Recent advances in research on carbon nanotube-polymer composites. Adv Mater 22(15):1672–1688
106. Yue L, Pircheraghi G, Monemian SA, Manas-Zloczower I (2014) Epoxy composites with carbon nanotubes and graphene nanoplatelets—Dispersion and synergy effects. Carbon NY 78:268–278
107. Bagotia N, Choudhary V, Sharma DK (2019) Synergistic effect of graphene/multiwalled carbon nanotube hybrid fillers on mechanical, electrical and EMI shielding properties of polycarbonate/ethylene methyl acrylate nanocomposites. Compos Part B Eng 159:378–388
108. Chen L et al (2014) Electron field emission characteristics of graphene/carbon nanotubes hybrid field emitter. J Alloys Compd 610:659–664
109. Liu F et al (2017) Investigation on the interfacial mechanical properties of hybrid graphene-carbon nanotube/polymer nanocomposites. Carbon NY 115:694–700
110. Zhang H et al (2018) Synergistic effect of carbon nanotube and graphene nanoplates on the mechanical, electrical and electromagnetic interference shielding properties of polymer composites and polymer composite foams. Chem Eng J 353:381–393
111. Li Y, Yang T, Yu T, Zheng L, Liao K (2011) Synergistic effect of hybrid carbon nantube-graphene oxide as a nanofiller in enhancing the mechanical properties of PVA composites. J Mater Chem 21(29):10844–10851
112. Hwang Y, Kim M, Kim J (2013) Improvement of the mechanical properties and thermal conductivity of poly(ether-ether-ketone) with the addition of graphene oxide-carbon nanotube hybrid fillers. Compos Part A Appl Sci Manuf 55:195–202

113. Kassab Z, El Achaby M, Tamraoui Y, Sehaqui H, Bouhfid R, Qaiss AEK (2019) Sunflower oil cake-derived cellulose nanocrystals: Extraction, physico-chemical characteristics and potential application. Int J Biol Macromol 136:241–252
114. Kassab Z, Boujemaoui A, Ben Youcef H, Hajlane A, Hannache H, El Achaby M (2019), Production of cellulose nanofibrils from alfa fibers and its nanoreinforcement potential in polymer nanocomposites. Cellulose 26(18):9567–9581
115. Calvino C, Macke N, Kato R, Rowan SJ (2020) Development, processing and applications of bio-sourced cellulose nanocrystal composites. Progr Polym Sci 103:101221 (Elsevier Ltd.)
116. Akindoyo JO, Ismail NH, Mariatti M (2019) Performance of poly(vinyl alcohol) nanocomposite reinforced with hybrid TEMPO mediated cellulose-graphene filler. Polym Test 80:106140
117. Ganjaee Sari M, Shamshiri M, Ramezanzadeh B (2017) Fabricating an epoxy composite coating with enhanced corrosion resistance through impregnation of functionalized graphene oxide-co-montmorillonite nanoplatelet. Corros Sci 129(September):38–53
118. He K et al (2019) Graphene hybridized polydopamine-kaolin composite as effective adsorbent for methylene blue removal. Compos Part B Eng 161:141–149
119. Zuo L et al (2017) Graphene/montmorillonite hybrid synergistically reinforced polyimide composite aerogels with enhanced flame-retardant performance. Compos Sci Technol 139:57–63
120. Zhou X et al (2018) Morphology and properties of shape memory thermoplastic polyurethane composites incorporating graphene-montmorillonite hybrids. J Appl Polym Sci 135(15):1–9
121. Wang R, Li Z, Liu W, Jiao W, Hao L, Yang F (2013) Attapulgite-graphene oxide hybrids as thermal and mechanical reinforcements for epoxy composites. Compos Sci Technol 87:29–35
122. Haase C, Tang F, Wilms MB, Weisheit A, Hallstedt B (2017) Combining thermodynamic modeling and 3D printing of elemental powder blends for high-throughput investigation of high-entropy alloys—Towards rapid alloy screening and design. Mater Sci Eng A 688:180–189
123. Huang K, Marthinsen K, Zhao Q, Logé RE (2018) The double-edge effect of second-phase particles on the recrystallization behaviour and associated mechanical properties of metallic materials. Progr Mater Sci 92:284–359 (Elsevier Ltd.)
124. Eaton P et al (2017) A direct comparison of experimental methods to measure dimensions of synthetic nanoparticles. Ultramicroscopy 182:179–190
125. Dudkiewicz A et al (2011) Characterization of nanomaterials in food by electron microscopy. TrAC Trends Anal Chem 30(1):28–43 (Elsevier)
126. Yang SY et al (2011) Synergetic effects of graphene platelets and carbon nanotubes on the mechanical and thermal properties of epoxy composites. Carbon NY 49(3):793–803
127. Zhang D, Chang H, Li P, Liu R, Xue Q (2016) Fabrication and characterization of an ultrasensitive humidity sensor based on metal oxide/graphene hybrid nanocomposite. Sens Actuat B Chem 225:233–240
128. Liang Y, Wang H, Casalongue HS, Chen Z, Dai H (2010) TiO_2 Nanocrystals grown on graphene as advanced photocatalytic hybrid materials. Nano Res 3(10):701–705
129. Wang J, Jin X, Wu H, Guo S (2017) Polyimide reinforced with hybrid graphene oxide @ carbon nanotube: toward high strength, toughness, electrical conductivity. Carbon NY 123:502–513
130. Kelly DJ et al (2018) Nanometer resolution elemental mapping in graphene-based TEM liquid cells. Nano Lett 18(2):1168–1174
131. Wang K, Ma Q, Pang K, Ding B, Zhang J, Duan Y (2018) One-pot synthesis of graphene/chitin nanofibers hybrids and their remarkable reinforcement on Poly(vinyl alcohol). Carbohydr Polym 194:146–153
132. Taj A et al (2019) In-situ synthesis of 3D ultra-small gold augmented graphene hybrid for highly sensitive electrochemical binding capability. J Colloid Interface Sci 553:289–297
133. Song S, Zhang Y (2017) Carbon nanotube/reduced graphene oxide hybrid for simultaneously enhancing the thermal conductivity and mechanical properties of styrene -butadiene rubber. Carbon NY 123:158–167

134. Chouhan DK et al (2016) Graphene oxide-Laponite hybrid from highly stable aqueous dispersion. Appl Clay Sci 132–133:105–113
135. Tajik S, Shahrabadi A, Rashidi A, Jalilian M, Yadegari A (2018) Application of functionalized silica-graphene nanohybrid for the enhanced oil recovery performance. Colloids Surfaces Physicochem Eng Asp 556:253–265
136. Swain SS, Unnikrishnan L, Mohanty S, Nayak SK (2019) Synergistic influence of anisotropic 3D carbon nanotube-graphene hybrid mixed matrix membranes on stability and gas permeation characteristics. J Taiwan Inst Chem Eng 105:150–165
137. Maya MG et al (2020) A comprehensive study on the impact of RGO/MWCNT hybrid filler reinforced polychloroprene rubber multifunctional nanocomposites. Polym Test 87:106525
138. Xiong R et al (2018) Wrapping nanocellulose nets around graphene oxide sheets. Angew Chemie Int Ed 57(28):8508–8513
139. Nanda SS, Yi DK, Kim K (2016) Study of antibacterial mechanism of graphene oxide using Raman spectroscopy. Sci Rep 6(1):1–12
140. Showalter AR, Duster TA, Szymanowski JES, Na C, Fein JB, Bunker BA (2017) An X-ray absorption fine structure spectroscopy study of metal sorption to graphene oxide. J Colloid Interface Sci 508:75–86
141. Viswanathan K, Ravi T, Boddula R (2019) Synthesis graphene based sensor for strain data and its characterization. Mater Sci Energy Technol 2(2):203–207
142. Ferrari AC, Basko DM (2013) Raman spectroscopy as a versatile tool for studying the properties of graphene. Nat Nanotechnol. 8(4):235–246
143. Bokobza L, Bruneel JL, Couzi M (2014) Raman spectroscopy as a tool for the analysis of carbon-based materials (highly oriented pyrolitic graphite, multilayer graphene and multiwall carbon nanotubes) and of some of their elastomeric composites. Vib Spectrosc 74:57–63
144. Hu X, Tian M, Qu L, Zhu S, Han G (2015) Multifunctional cotton fabrics with graphene/polyurethane coatings with far-infrared emission, electrical conductivity, and ultraviolet-blocking properties. Carbon NY 95:625–633
145. Mahendia S, Heena, Kandhol G, Deshpande UP, Kumar S (2016) Determination of glass transition temperature of reduced graphene oxide-poly(vinyl alcohol) composites using temperature dependent Fourier transform infrared spectroscopy. J Mol Struct 1111:46–54
146. Sajith S (2019) Investigation on effect of chemical composition of bio-fillers on filler/matrix interaction and properties of particle reinforced composites using FTIR. Compos Part B Eng 166:21–30
147. Costa P et al (2017) High-performance graphene-based carbon nanofiller/polymer composites for piezoresistive sensor applications. Compos Sci Technol 153:241–252
148. Pu X et al (2013) One-pot microwave-assisted combustion synthesis of graphene oxide-TiO_2 hybrids for photodegradation of methyl orange. J Alloys Compd 551:382–388
149. Han Y, Liu Y, Han L, Lin J, Jin P (2017) High-performance hierarchical graphene/metal-mesh film for optically transparent electromagnetic interference shielding. Carbon NY 115:34–42
150. Xu Y et al (2009) A hybrid material of graphene and poly (3,4-ethyldioxythiophene) with high conductivity, flexibility, and transparency. Nano Res 2(4):343–348
151. Wang P, Han L, Zhu C, Zhai Y, Dong S (2011) Aqueous-phase synthesis of Ag–TiO_2-reduced graphene oxide and Pt-TiO_2-reduced graphene oxide hybrid nanostructures and their catalytic properties. Nano Res 4(11):1153–1162
152. Vaghri E, Khalaj Z, Dorranian D (2020) Investigating the effects of different liquid environments on the characteristics of multilayer graphene and graphene oxide nanosheets synthesized by green laser ablation method. Diam Relat Mater 103:107697
153. Das S et al (2011) Synthesis and characterization of self-organized multilayered graphene-carbon nanotube hybrid films. J Mater Chem 21(20):7289–7295
154. Xu H et al (2018b) Properties of graphene-metal contacts probed by Raman spectroscopy. Carbon NY 127:491–497
155. Dey A et al (2015) Polymer based graphene/titanium dioxide nanocomposite (GTNC): an emerging and efficient thermoelectric material. Dalt Trans 44(44):19248–19255

156. Hasan M, Banerjee AN, Lee M (2015) Enhanced thermo-optical performance and high BET surface area of graphene@PVC nanocomposite fibers prepared by simple facile deposition technique: N_2 adsorption study. J Ind Eng Chem 21:828–834
157. Zhan Y, Zhang J, Wan X, Long Z, He S, He Y (2018) Epoxy composites coating with Fe_3O_4 decorated graphene oxide: modified bio-inspired surface chemistry, synergistic effect and improved anti-corrosion performance. Appl Surf Sci 436:756–767
158. Greczynski G, Hultman L (2020) X-ray photoelectron spectroscopy: towards reliable binding energy referencing. Progr. Mater. Sci 107:100591 (Elsevier Ltd.)
159. Tajik S, Nasernejad B, Rashidi A (2016) Preparation of silica-graphene nanohybrid as a stabilizer of emulsions. J Mol Liq 222:788–795
160. Zheng Q, Cai Z, Ma Z, Gong S (2015) Cellulose nanofibril/reduced graphene oxide/carbon nanotube hybrid aerogels for highly flexible and all-solid-state supercapacitors. ACS Appl Mater Interfaces 7(5):3263–3271
161. Tan QC, Shanks RA, Hui D, Kong I (2016) Functionalised graphene-multiwalled carbon nanotube hybrid poly(styrene-b-butadiene-b-styrene) nanocomposites. Compos Part B Eng 90:315–325
162. Dai W et al (2015) Enhanced thermal conductivity and retained electrical insulation for polyimide composites with SiC nanowires grown on graphene hybrid fillers. Compos Part A Appl Sci Manuf 76:73–81